A high-resolution mRNA expression time course of embryonic development in zebrafish

Richard J. White[1], John E. Collins[1], Ian M. Sealy[1], Neha Wali[1], Christopher M. Dooley[1], Zsofia Digby[1,3], Derek L. Stemple[1], Daniel N. Murphy[2], Thibaut Hourlier[2], Anja Füllgrabe[2], Matthew P. Davis[2], Anton J. Enright[2] and Elisabeth M. Busch-Nentwich[1†]

[1]Wellcome Trust Sanger Institute, Wellcome Genome Campus, Hinxton, CB10 1HH, UK

[2]EMBL-European Bioinformatics Institute, Wellcome Genome Campus, Hinxton, CB10 1SD, UK

[3]Current address: Department of Veterinary Medicine, Madingley Road, Cambridge, CB3 0ES, UK

[†]Author for correspondence, emb@sanger.ac.uk

Abstract

We have produced an mRNA expression time course of zebrafish development across 18 time points from 1-cell to 5 days post-fertilisation sampling individual and pools of embryos. Using poly(A) pulldown stranded RNA-seq and a 3′ end transcript counting method we characterise the temporal expression profiles of 23,642 genes. We identify temporal and functional transcript co-variance that associates 5,024 unnamed genes with distinct developmental time points. Specifically, a class of over 100 previously uncharacterised zinc finger domain containing genes, located on the long arm of chromosome 4, is expressed in a sharp peak during zygotic genome activation. The data reveal complex and widespread differential use of exons and previously unidentified 3′ ends across development, new primary microRNA transcripts and temporal divergence of gene paralogues generated in the teleost genome duplication. To make this dataset a useful baseline reference, the data are accessible to browse and download at Expression Atlas and Ensembl.

Keywords

Developmental biology, embryogenesis, RNA-seq, transcriptome, zebrafish.

Introduction

Gene regulatory interactions are the fundamental basis of embryonic development and transcription is one of the major processes by which these interactions are mediated. A time-resolved comprehensive analysis of relative mRNA expression levels is an important step towards understanding the regulatory processes governing embryonic development. Here we present a systematic assessment of the temporal transcriptional events during this critical period in zebrafish (*Danio rerio*).

The zebrafish is a unique vertebrate model system as it possesses high morphological and genomic conservation with humans, but also experimental tractability of embryogenesis otherwise only found in invertebrate model organisms such as *Drosophila melanogaster* or *Caenorhabditis elegans*. Features such as very large numbers of offspring, *ex vivo* development and embryonic translucency have enabled comprehensive forward and reverse genetic screens (Amsterdam et al., 1999; Driever et al., 1996; Haffter et al., 1996; Kettleborough et al., 2013; Moens et al., 2008; Varshney et al., 2015) as well as high-throughput drug discovery approaches (Murphey et al., 2006; North et al., 2007; Peterson et al., 2000; Peterson et al., 2004; Stern et al., 2005). Together with a high quality genome (Howe et al., 2013b) only comparable in vertebrates to mouse and human, this has led to many important discoveries in areas such as zygotic genome activation (ZGA)(Lee et al., 2013), blood stem cell biology (Bertrand et al., 2010; Kissa and Herbomel, 2010), but also highly translational findings directly affecting human health (Li et al., 2015; Tobin et al., 2010).

The morphological processes underlying the transformation of a fertilised egg into a free swimming fish have been studied extensively owing to the ease with which embryogenesis can be observed and manipulated (Behrndt et al., 2012). This has identified many genes that drive crucial steps of the differentiation process, however the wealth of morphological phenotype data has not been matched with a systematic analysis of the corresponding molecular events. Baseline transcriptomic datasets in other species have greatly improved knowledge of relative levels of gene expression

as well as alternative splicing events (Boeck et al., 2016; Brown et al., 2014; Gerstein et al., 2014; Graveley et al., 2011; Hashimshony et al., 2015; Klepikova et al., 2016; Owens et al., 2016; Tan et al., 2013).

Previous baseline transcriptome work in zebrafish has focused on either certain aspects of development such as the maternal-zygotic transition (Aanes et al., 2011; Harvey et al., 2013; Lee et al., 2013), the identification of specific transcript types (Pauli et al., 2012) or promoters (Gehrig et al., 2009; Nepal et al., 2013), on gene annotation improvement (Collins et al., 2012) or have a limited number of time points and replicates (Yang et al., 2013).

Using poly(A) pulldown RNA-seq and a 3′ end enrichment method called DeTCT (Collins et al., 2015) we have generated a comprehensive polyadenylated RNA expression profile of normal zebrafish development. We have taken advantage of the large numbers of offspring and have divided the 6 day period of embryonic development into 18 stages. For each stage we have processed up to 29 biological replicates consisting of single or pooled embryos.

We have placed particular emphasis on making the presented data accessible without the need for computational processing. The data are available to browse and download in a user-friendly interface at Expression Atlas and as selectable tracks in the Ensembl genome browser. Furthermore, incorporation into the next Ensembl gene set update will significantly improve zebrafish gene and transcript isoform annotation.

This developmental polyadenylated RNA baseline reference enhances our understanding of the gene regulatory events during vertebrate development and provides a time-resolved transcriptional basis for the comprehensive annotation of functional elements in the zebrafish genome using existing and future genome-wide datasets (Haberle et al., 2014; Kaaij et al., 2016; Lindeman et al., 2010; Potok et al., 2013; Vastenhouw et al., 2010).

Results

A high-resolution transcriptional profile of zebrafish development

A total of 18 developmental time points were sampled in this study (Figure 1A). Four time points are before or at the onset of zygotic transcription, four during gastrulation, three during somitogenesis, three during prim stages – 24, 30 and 36 hours post-fertilisation (hpf) – and every 24 h from 2 to 5 days post-fertilisation (dpf). This gives detailed coverage of all the important developmental processes taking place during this time period. At each time point, samples were collected for both RNA-seq and DeTCT (RNA-seq, pools of 12 embryos, 5 replicates; DeTCT, pools of 8 embryos, 11-12 replicates and individual embryos, 11-12 replicates). We obtained an average of 3.8 million reads per sample for the RNA-seq and 9 million reads per sample for the DeTCT data (Figure 1B). The number of genes detected rises steadily as development proceeds and a wider range of genes are expressed (Figure 1C, Supplemental Figure 1-1). With a cut-off of greater than or equal to 5 normalised counts it rises from a mean of 10,395 to 18,225 for the RNA-seq (6,259 to 15,215 in the DeTCT data).

For quality control purposes, counts from the RNA-seq data, normalised for library size, were first used to produce a sample correlation matrix (Figure 1D). This shows the excellent agreement among biological replicates and close relation of neighbouring stages in terms of gene expression profiles. To give a high level overview of the data, principal component analysis (PCA) was used to visualise patterns. These show close clustering of biological replicates and a smooth transition from one stage to another through developmental time. The first six principal components (PCs) explain just over 90% of the variance in the data (Figure 1E-G and Supplemental Figure 1-2); the first component accounts for 58.2% of the observed variation. Summaries of the expression patterns underlying the PCs are shown in Figure 1H. Broadly, the genes that contribute the most to the first PC are either low at early time points and increase towards the end of the time course or the inverse (high early and decreasing later). PC2 represents genes with a peak at gastrula and somite stages. Genes contributing to PC3 show two peaks of

119 expression (onset of transcription and days 3-5). The other patterns are more
120 complex (Supplemental Figure 1-2) although PC6 shows a clear spike of expression
121 starting at the 1000-cell stage (3 hpf), which coincides with the start of zygotic
122 transcription.

123 In order for this dataset to be as useful as possible to the scientific community, we
124 have made it available as sequence with metadata through the European Read
125 Archive and in multiple locations for viewing. Pre-computed count profiles (FPKM)
126 are available to search/browse at Expression Atlas
127 (http://www.ebi.ac.uk/gxa/experiments/E-ERAD-475)(Petryszak et al., 2016),
128 allowing comparison of the expression profiles of multiple genes across the entire
129 time course (Figure 2A). This is searchable by gene/allele name, Ensembl/ZFIN ID
130 and GO terms. It is also possible to start with a single seed gene and have
131 Expression Atlas add in similarly expressed genes (as assessed by k-means
132 clustering) for comparison (https://www.ebi.ac.uk/gxa/FAQ.html#similarExpression).
133 The data are also viewable in Ensembl as separate stage-specific selectable tracks
134 along with one merged track (http://www.ensembl.org/Danio_rerio). The aligned
135 reads can be displayed as either coverage graphs or read pairs. Reads that span
136 introns can be viewed to investigate alternative splicing in a stage-specific manner
137 (Figure 2B-C).

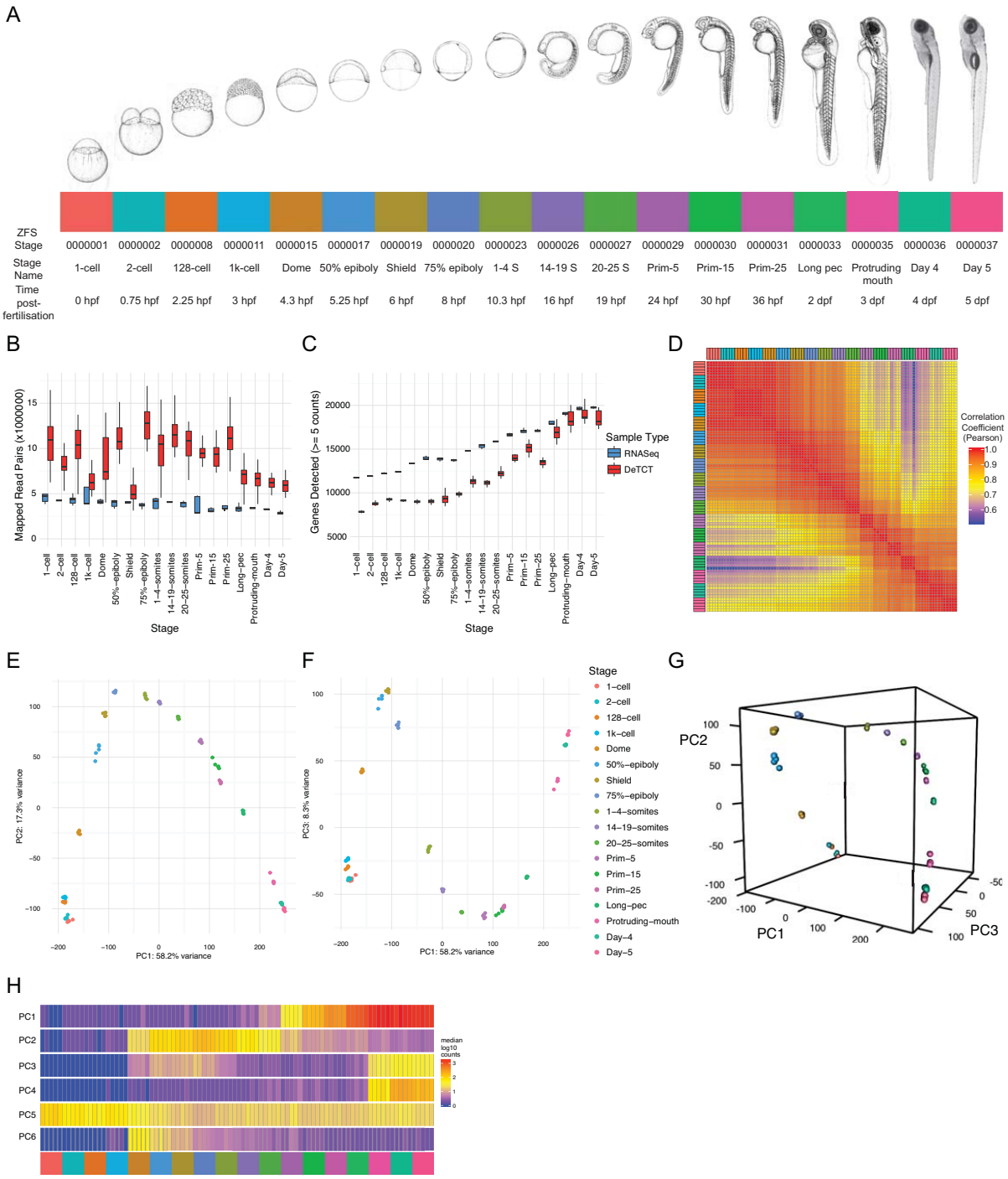

Figure 1. A transcriptional map of development. (A) Stages represented in this study. Images of embryos from 1-cell to protruding mouth are from (Kimmel et al., 1995). (B-C) Boxplot showing the distributions of numbers of mapped read-pairs and genes detected for each stage and protocol. (D) Sample correlation matrix showing the Pearson correlation coefficient between all pairwise combinations of samples. (E-G) Principal Component Analysis. (E) Principal Component (PC) 2 plotted against PC1. (F) PC3 plotted against PC1. (G) 3D rendering of the first 3 PCs. (H) Representation of expression profiles contributing to the first 6 PCs, produced by

calculating the median expression value (normalised counts) for each sample for the 100 genes that contribute most to that PC.

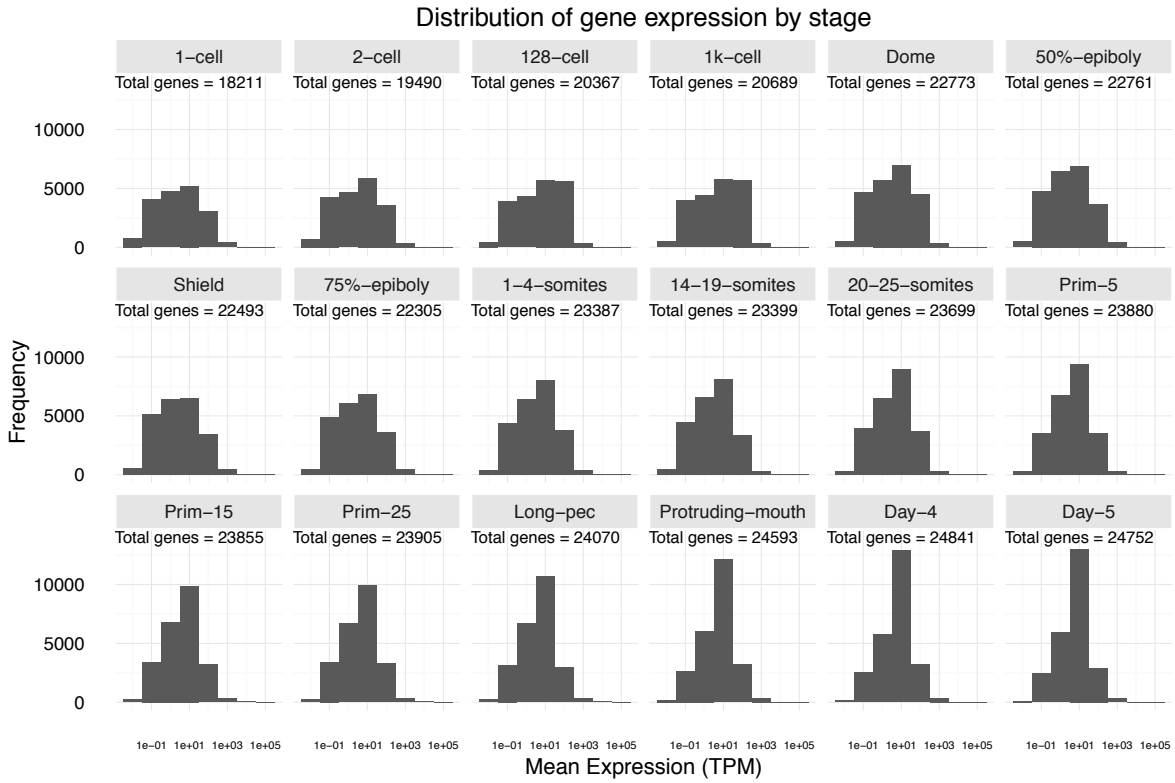

Figure1-1. Distribution of gene expression levels in RNA-seq data by stage. Histograms (one per stage) showing the distribution of the mean expression level for each gene over the 5 samples within the stage. The total number of genes represented for the stage is shown on each panel.

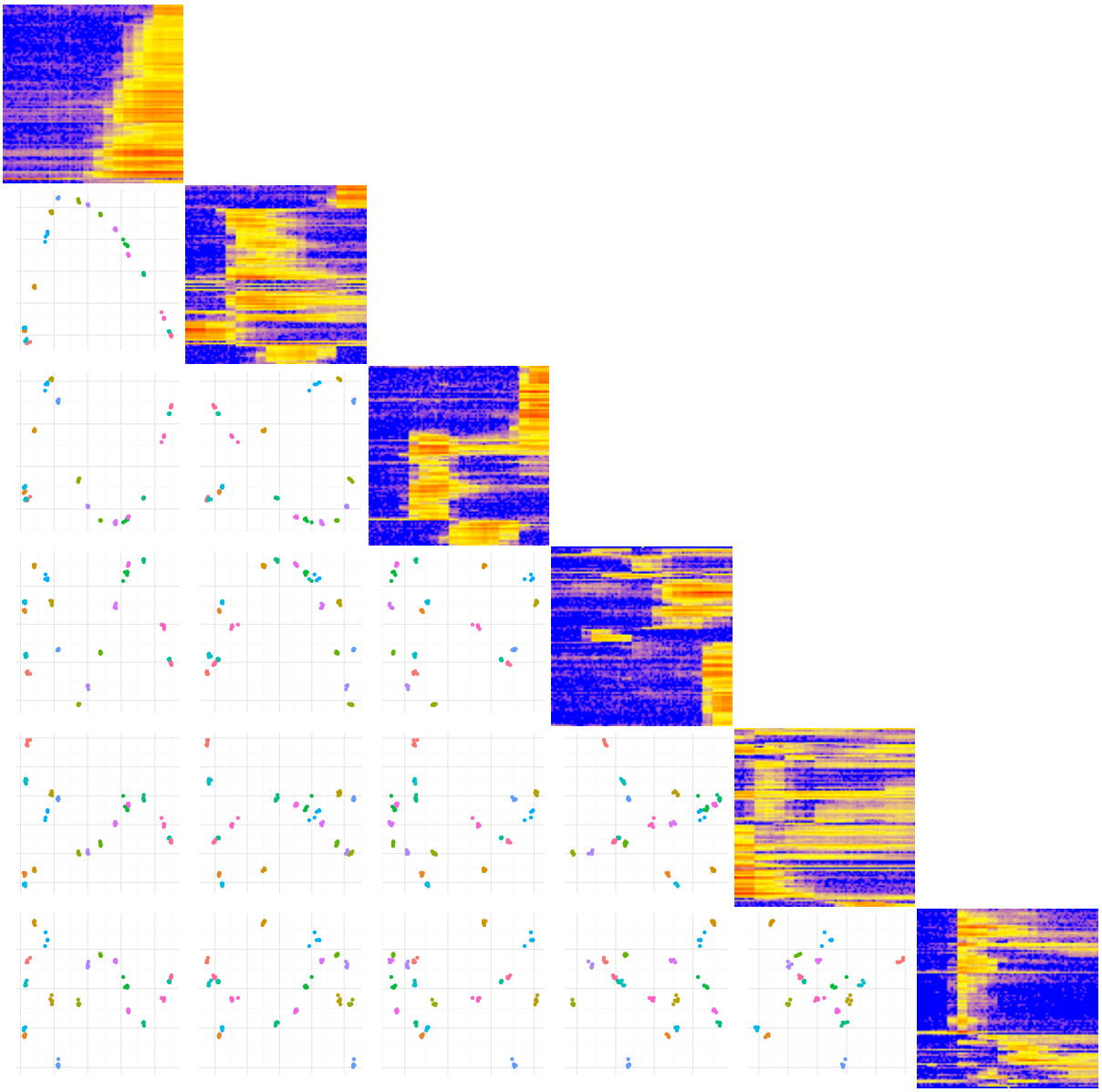

Figure1-2. Matrix PCA plot. Plots showing the first six principal components (PCs) plotted against each other. The components are arranged in a matrix from PC1 (top and left) to PC6 (bottom and right). The plots on the diagonal show the expression profiles of the 100 genes contributing the most to that component. The plots below the diagonal show the appropriate PCs plotted against each other. For example, the plot in the third row and first column is PC1 (x-axis) plotted against PC3 (y-axis).

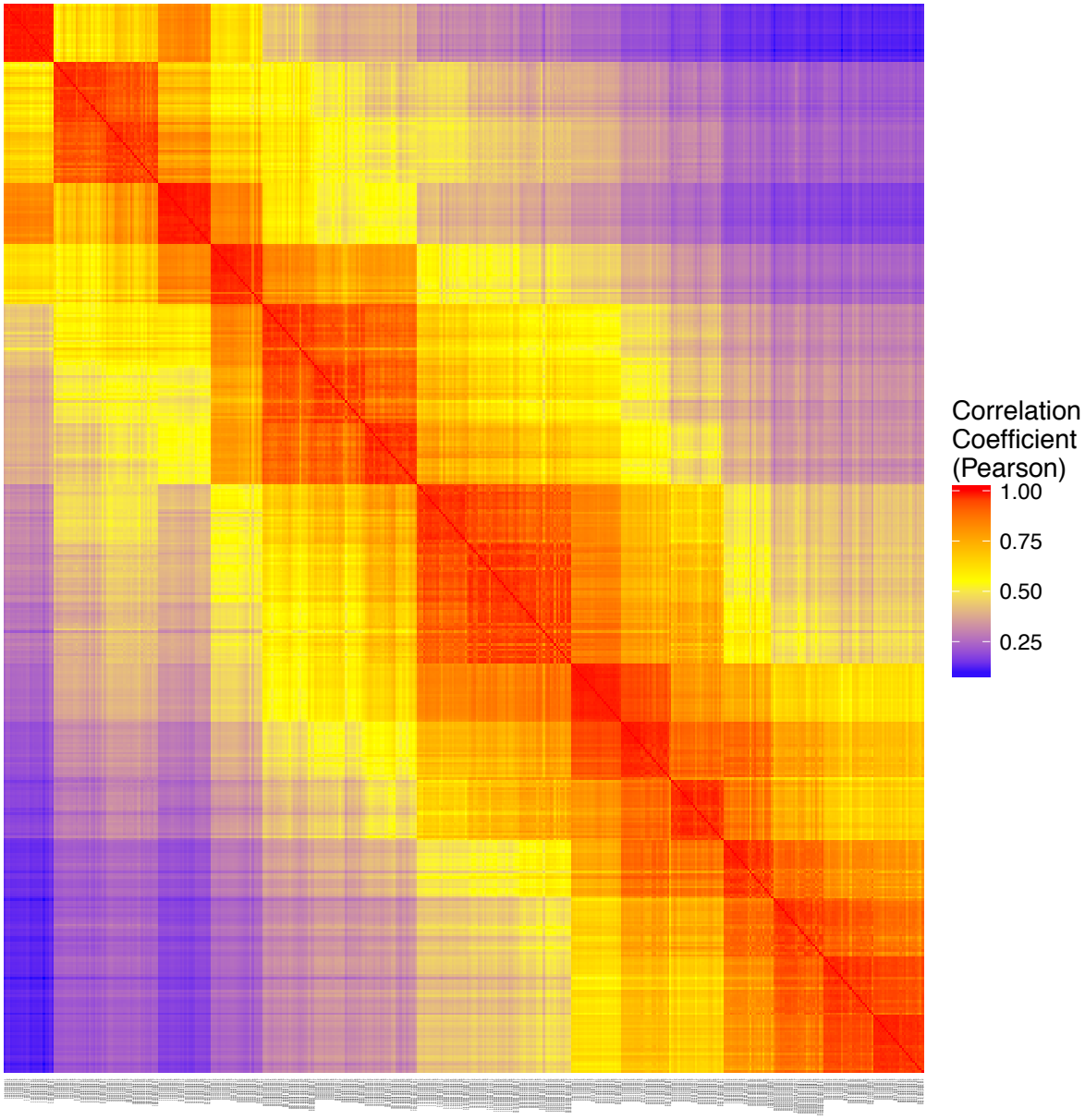

Figure1-3. DeTCT sample Correlation matrix. Sample correlation matrix showing the Pearson correlation coefficient between each pair-wise comparison of samples**.**

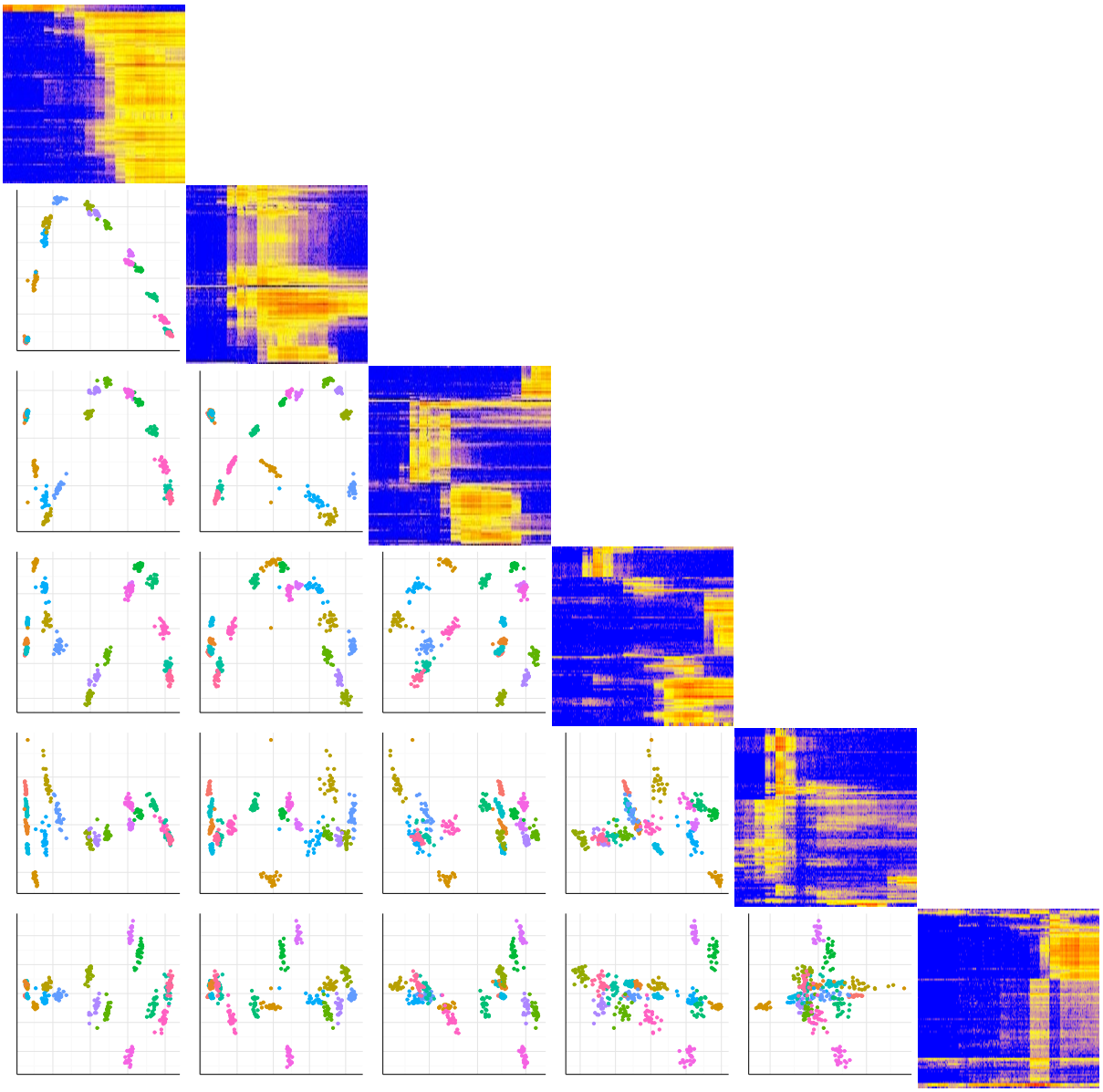

Figure1-4. DeTCT Matrix PCA plot. Plot showing the PCA of the DeTCT data arranged in the same way as Figure 1-2.

A

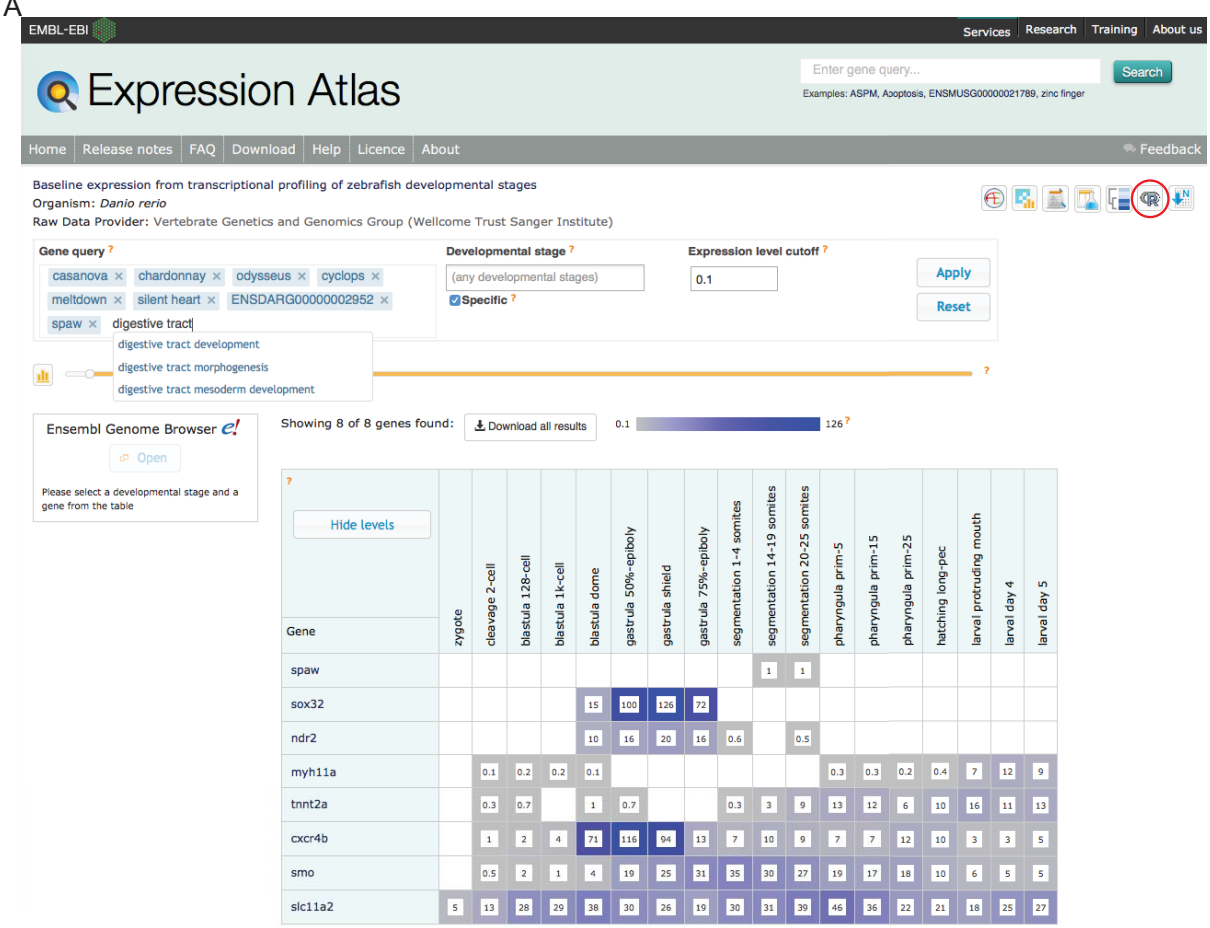

B

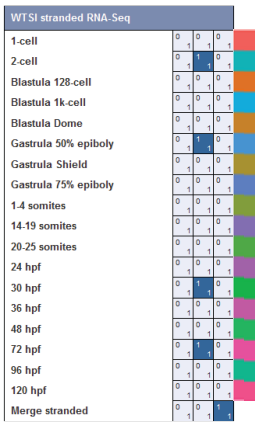

C

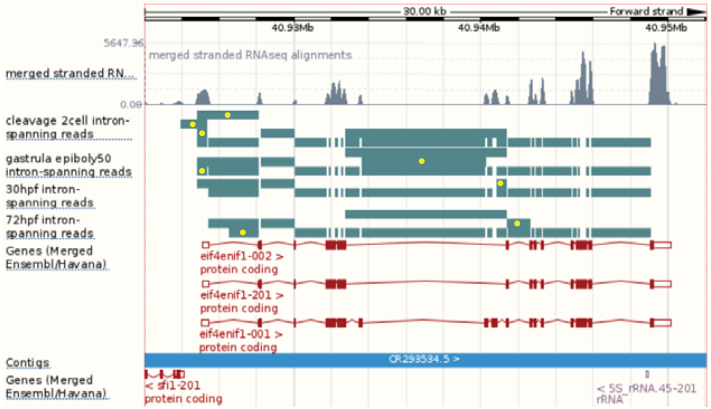

Figure 2. Data Access. (A) A screenshot from Expression Atlas release Dec 2016. Relative gene expression levels across all 18 stages are shown in FPKM. Genes can be searched for using Ensembl IDs, ZFIN gene IDs, gene/allele names and Gene Ontology terms. The data for the selected genes can be downloaded (red circle) as can the entire dataset. (B) A screenshot of Ensembl v87 showing the RNA-seq matrix with four intron tracks plus the merged RNA-seq data from exon read coverage from all 18 stages chosen for display. (C) A screenshot of Ensembl v87

showing the region surrounding the gene *eif4enif1* (chr 6:40.922-40.952 Mb). Exon read coverage from the merged 18 stages is shown as grey histograms. Four of the 18 intron-defining tracks from the RNA-seq matrix are shown. Introns are coloured in teal. Yellow dots indicate introns identifying a splice variant not shown by any of the three gene models shown in red. Note only the forward strand is shown in full and a gene model overlaps on the reverse strand.

Temporal Map of Development

To visualise the expression of all genes across development we ordered the genes in our dataset by their stage of maximum expression (Figure 3A). This organises the genes temporally, broadly by expression pattern. These 18 groups of genes were then analysed for enrichment of Zebrafish Anatomy Ontology (ZFA) and Gene Ontology (GO) terms.

ZFA enrichment

The Zebrafish Anatomy Ontology (ZFA, Van Slyke et al., 2014) is a controlled vocabulary for describing the anatomy and development of zebrafish and is used by the zebrafish model organism database (ZFIN Howe et al., 2013a) to annotate the spatial expression patterns of genes from the literature and large-scale whole mount mRNA *in situ* hybridisation experiments (Rauch et al., 2003; Thisse et al., 2001). The results show enrichments for cell types and tissues that are appropriate to the stages of maximum expression (Figure 3A). There are no significant enrichments of terms during cleavage stages. At early gastrula stages terms such as hypoblast, organiser and hatching gland are enriched with endoderm, yolk and epidermis being enriched at late gastrula. During segmentation stages terms such as muscle, notochord and haematopoietic system are enriched and then at pharyngula and larval stages terms associated with the nervous system and the neural crest become enriched. By contrast, terms for mesodermal and endodermal organs such as kidney, spleen and liver are enriched at later stages (days 4 and 5). This demonstrates that these groupings of genes are consistent with what is already known about zebrafish development, thus validating our dataset.

GO enrichment

Enrichment analysis using the Gene Ontology (GO) also shows enrichments of terms in a stage-appropriate manner. At cleavage stages, terms linked to cell division, DNA repair, protein turnover and chromatin modification are enriched, consistent with the fast rate of cell division as well as the large changes in chromatin structure that occur at early stages. Subsequently, terms associated with determination of the embryonic axes and specification of the major tissue divisions are enriched. For example, genes linked to anterior-posterior, dorsal-ventral and left-right patterning are enriched from dome until prim-25 as well as genes annotated to terms such as gastrulation, heart development, muscle cell differentiation and brain development. At later stages, more specific terms such as synaptic transmission, potassium ion transport and glutamate receptor signalling are enriched. Coordinated expression of blood clotting factor genes leads to the appearance of blood coagulation as an enriched term at day 4.

Of the 23,642 genes 5,024 are uncharacterised (i.e. genes with automatically generated names such as zgc:* and si:ch*). Interestingly, at dome and gastrula stages, the proportion of these unnamed genes is much higher (29.2-39.4%) than at other stages (14.4-26.5%; Figure 3A). This could indicate a lack of orthologues and therefore that zebrafish gastrulation is enriched for the expression of genes exclusive to this species. However, we looked at the proportions of unnamed genes with orthologues in various species. Genes with no orthologues in any of the species were categorised as Danio, those with orthologues present in the fish species examined, but not the mammals were termed Teleost and those with orthologues present in the mammals as well were termed Vertebrate (although in many cases the identified last common ancestor is more basal than vertebrates e.g. Bilateria). The proportions of these categories are broadly constant across all 18 stages and there is not an increase of the Danio-specific genes at gastrulation (Supplemental Figure 3-1). This suggests that there is a large number of genes involved in vertebrate gastrulation that are yet to be characterised. The complete list of clusters along with the ZFA/GO term enrichment are provided in Supplemental Data Files 3-5.

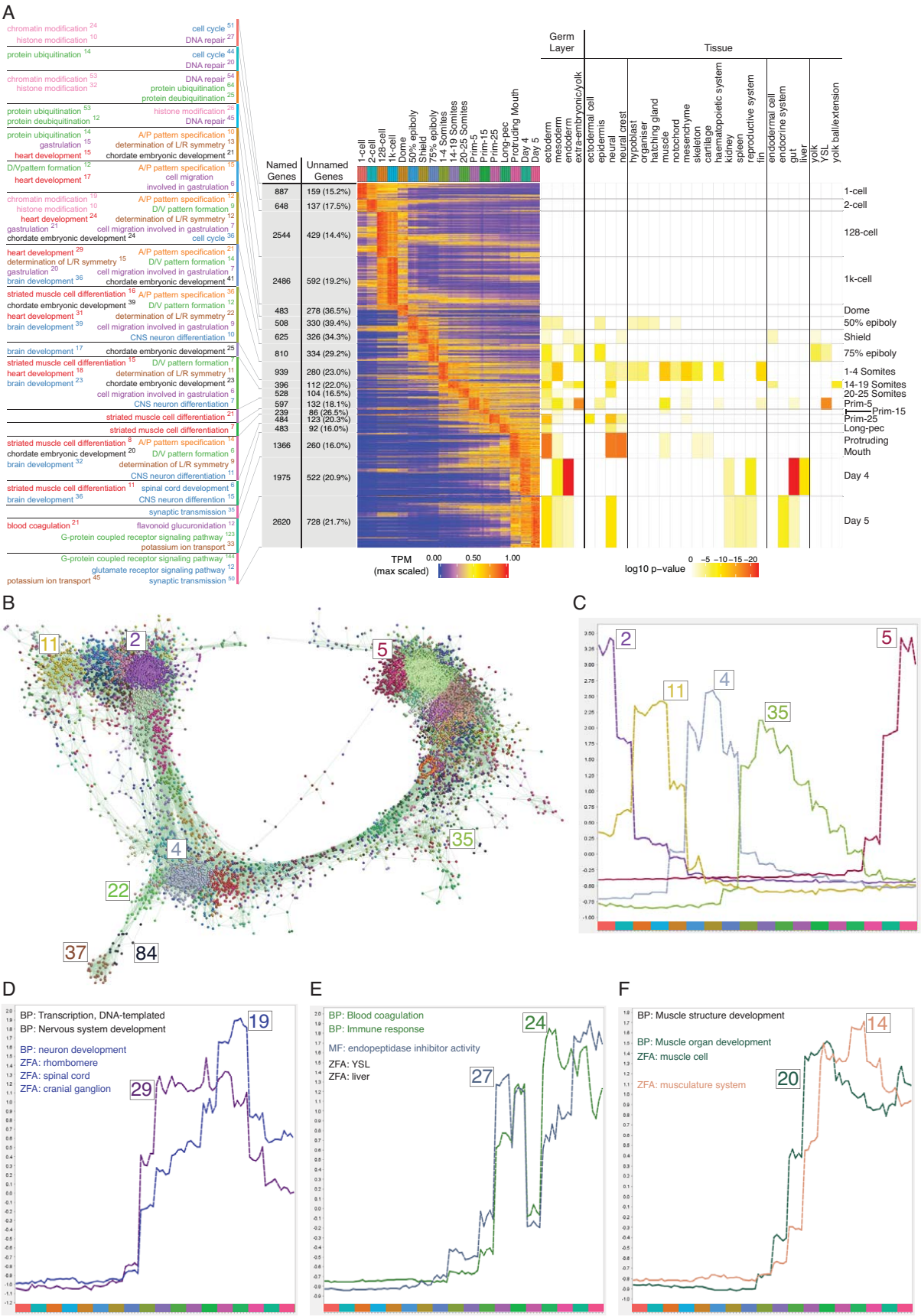

Figure 3. Clustering of expression patterns. (A) Heatmap showing the expression profiles of all the genes with appreciable expression in at least one stage. The

expression values (Transcripts per Million, TPM) are scaled to the maximum expression for that gene across the time course and genes are organised by which stage the maximum expression occurs at. To the right is a heatmap of ZFA enrichments based on the genes assigned to each stage. To the left are a selection of the GO enrichments. The numbers of genes assigned to each GO term are shown as superscripts. Also shown are the numbers of named and unnamed genes assigned to each stage. (B) Network diagram showing the clustering produced by MCL on a network graph generated by linking genes that have at least one sample with 6 or more normalised counts, a Pearson correlation coefficient of > 0.94 and removing clusters with five genes or fewer. The numbers show the positions in the network diagram of the clusters shown in C and the ZnF clusters shown in Figure 4. (C-F) Example expression profiles displayed as lines showing the mean of mean-centred and variance-scaled normalised counts. (C) Example clusters showing the progression of expression peaks through development. (D-F) Expression profiles of example clusters with interesting GO/ZFA enrichments. Terms in black apply to all clusters in the diagram whereas terms specific to one cluster are shown in that colour.

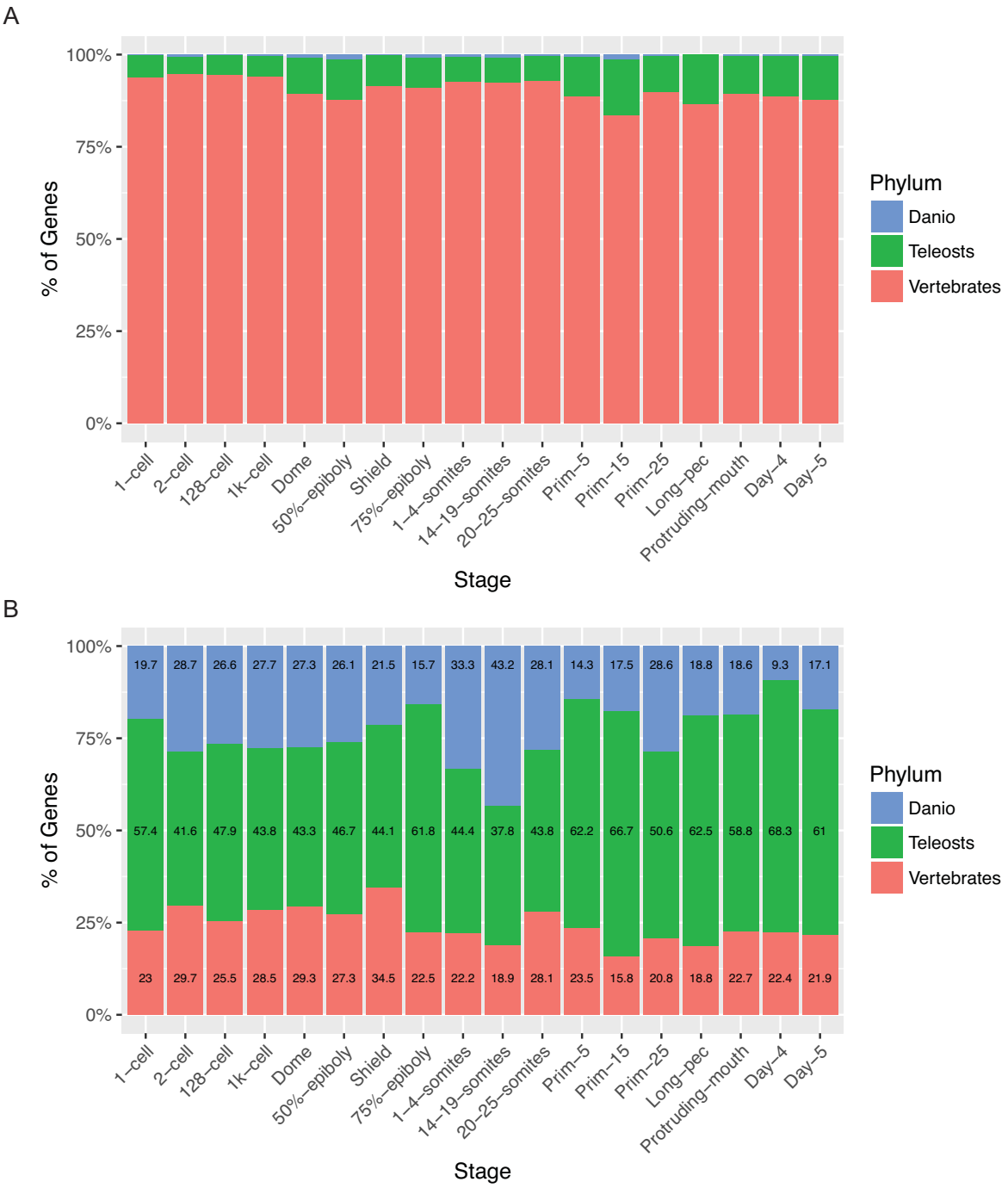

Figure 3-1. Relationship of named and unnamed genes to other species. Stacked bar charts showing the proportions of genes with orthologues at different taxonomic levels for Named (A) and Unnamed (B) genes. Orthologues for genes were obtained from the Ensembl Compara database and genes were then categorised based on which species they have orthologues in. Genes with no identifiable orthologue in any of the species examined were classed as *Danio* specific (top bar, blue). Those with orthologues in the six fish species (*Astyanax mexicanus*, *Gasterosteus aculeatus*, *Oryzias latipes*, *Takifugu rubripes*, *Tetraodon*

266 *nigroviridis*, *Gadus morhua*), but not the mammals examined were labelled Teleosts
267 (middle bar, green). Those with orthologues also present in the mammals surveyed
268 (*Mus musculus*, *Rattus norvegicus* and *Homo sapiens*) were labelled Vertebrates
269 (bottom bar, red).

270 Graph-based clustering produces compact clusters of 271 highly biologically related genes

272 While the maximum expression stage groupings provide a high-level, temporally
273 organised view of development, smaller more specific groupings would provide more
274 insight especially into the role of uncharacterised genes. To get smaller clusters that
275 are more likely to be highly biologically related we used the BioLayout *Express*^{3D}
276 software (http://www.biolayout.org/) (Theocharidis et al., 2009) to cluster and
277 visualise the dataset (Figure 3B). The software first builds a network graph in which
278 genes are nodes with edges between those whose expression is correlated above a
279 given threshold. It then uses the Markov Cluster Algorithm (MCL, Enright et al.,
280 2002; van Dongen, 2000) to find strongly connected components within the graph.
281 These are clusters of genes that are more highly connected with each other than
282 with the rest of the graph. This produces 252 clusters, the vast majority of which
283 (238) have fewer than 100 genes (Figure 3B). Broadly speaking, the clusters on the
284 left-hand side of the graph represent genes expressed at early stages, whereas
285 towards the right of the graph the expression profiles are progressively later in
286 development (Figure 3B-C). For example, cluster 2 contains genes that are
287 maternally supplied and then degraded, cluster 11 has genes that accumulate after
288 the 2-cell stage (possibly by control of polyadenylation) and are then cleared. To test
289 whether this is an artefact of the normalisation process, we also normalised the
290 counts using the ERCC spike-in RNAs included in every sample. The expression
291 profiles are similar, although the ERCC normalisation introduces more variability
292 from embryo to embryo within the same stage (Figure 3-2). After the maternal
293 stages, cluster 4 genes are expressed at the time of zygotic genome activation,
294 cluster 35 genes are expressed during segmentation stages and genes from cluster
295 5 are not expressed until the last time points in the study (Figure 3C).

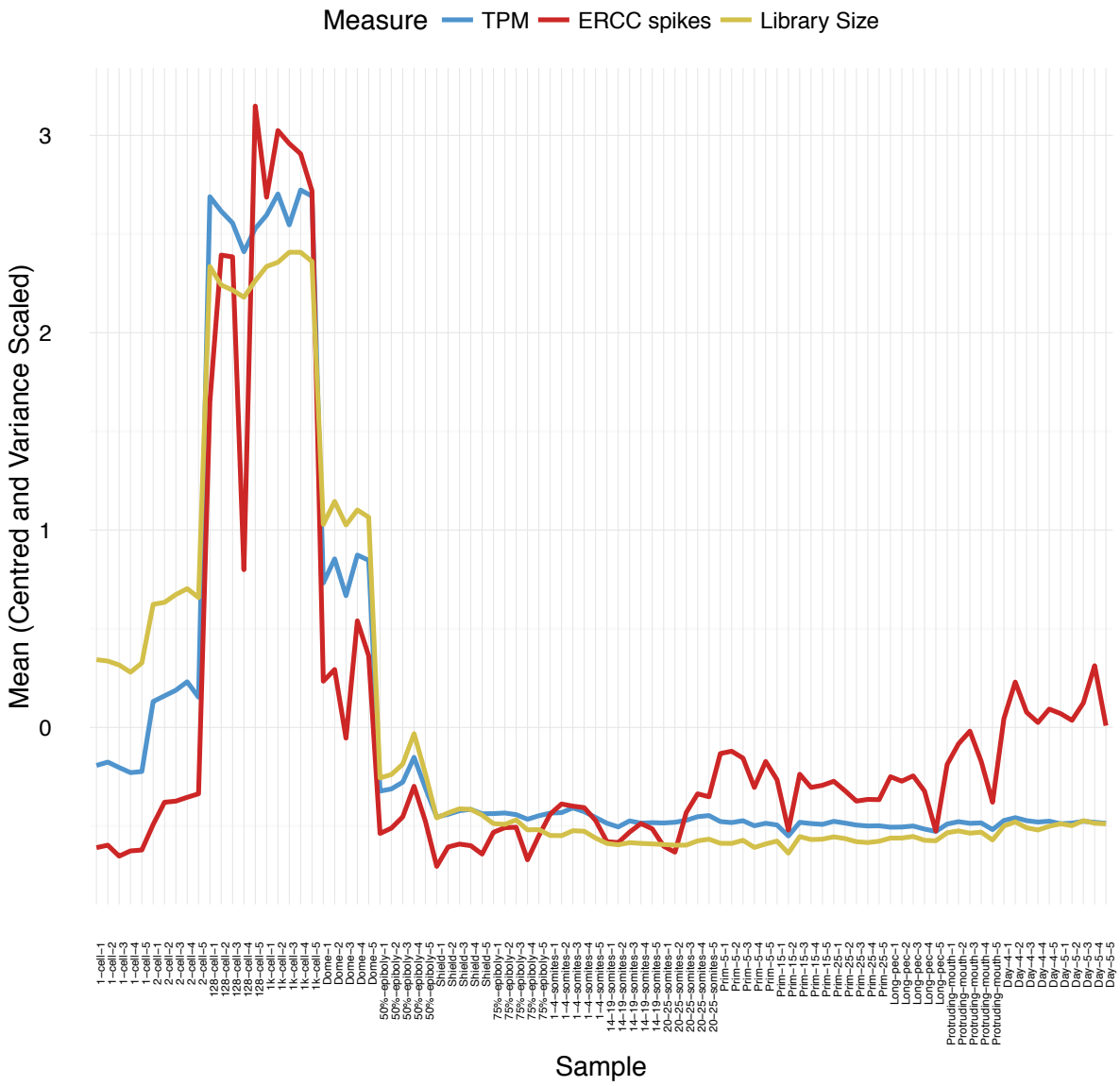

Figure 3-2. Effect of normalisation on expression profile of cluster 11 genes. Counts were normalised by DESeq2 using either the ERCC spike-in RNAs (ERCC spikes, red line) or all the counts for each sample (Library size, yellow line). As a comparison, TPM is also shown (blue line).

We again used GO and ZFA enrichment to analyse the composition of the genes within the clusters. For example, cluster 19 contains large numbers of transcription factors from the *dlx*, *hox*, *irx* and *pax* gene families that are expressed from 1-4 somites onwards and is associated with GO terms for transcription and nervous system development and ZFA terms such as rhombomere, spinal cord and cranial ganglion (Figure 3D). Cluster 29, with similar GO enrichments, has an overlapping

308 expression profile but an earlier and broader peak. It contains genes such as *nkx2.1*,
309 *gli3*, *sox1b* and *hoxb* genes. Clusters 24 and 27 show a sharp dip in expression at
310 36 hpf and contain complement, clotting factor genes and serpins. Both clusters
311 have significant enrichments for the terms blood coagulation and endopeptidase
312 inhibitor activity (Figure 3E). (Figure 3F). The information on cluster assignments and
313 GO/ZFA enrichments are provided in Supplemental Data Files 6-9.

314 A burst of transcription of highly related zinc finger
315 proteins during zygotic genome activation

316 During examination of the clusters produced by BioLayout, we noticed several
317 clusters that appeared to be enriched for a family of zinc finger (ZnF) proteins
318 located on chromosome 4 (Howe et al., 2016). To test systematically if any
319 chromosomes were over-represented in any of the clusters, we performed a binomial
320 test for each chromosome for each cluster that contained more than five genes from
321 that chromosome. Table 1 shows the clusters and chromosomes that are
322 significantly enriched by more than twofold. This identifies four clusters (Figure 3B,
323 clusters 4, 22, 37 and 84) with more chromosome 4 genes than would be expected
324 by chance given the size of the clusters. Most of the chromosome 4 genes within
325 these clusters are predicted to encode proteins with ZnF domains (Supplemental
326 Data File 10).

327 The expression profiles of these ZnF genes show a burst of expression from dome to
328 75% epiboly (4.3-8 hpf) and several of them show appreciable RNA levels at the
329 128- and 1000-cell stages (Figure 4A-B, Supplemental Figure 4-1). Cluster 37 shows
330 a particularly sharp peak with a very large increase from the 1000-cell stage to dome
331 and an almost equal decrease from dome to 50% epiboly. This suggests that these
332 ZnF genes are co-ordinately expressed at the onset of zygotic transcription. To
333 investigate whether this is a global effect on all the genes on the long arm of
334 chromosome 4 we looked at the expression profiles of NLR family genes, another
335 large family of proteins present on chromosome 4. These genes are present in the
336 same region of chromosome 4 as the ZnF genes although their distribution is slightly
337 different, with more NLR genes towards the end of the chromosome (Figure 4F-G,
338 Supplemental Figure 4-2). Of the 312 NLR genes present in the Ensembl version 85

339 genebuild, 149 have appreciable expression during this time course and they are not
340 expressed in the same pattern as the ZnF genes (Figure 4C).

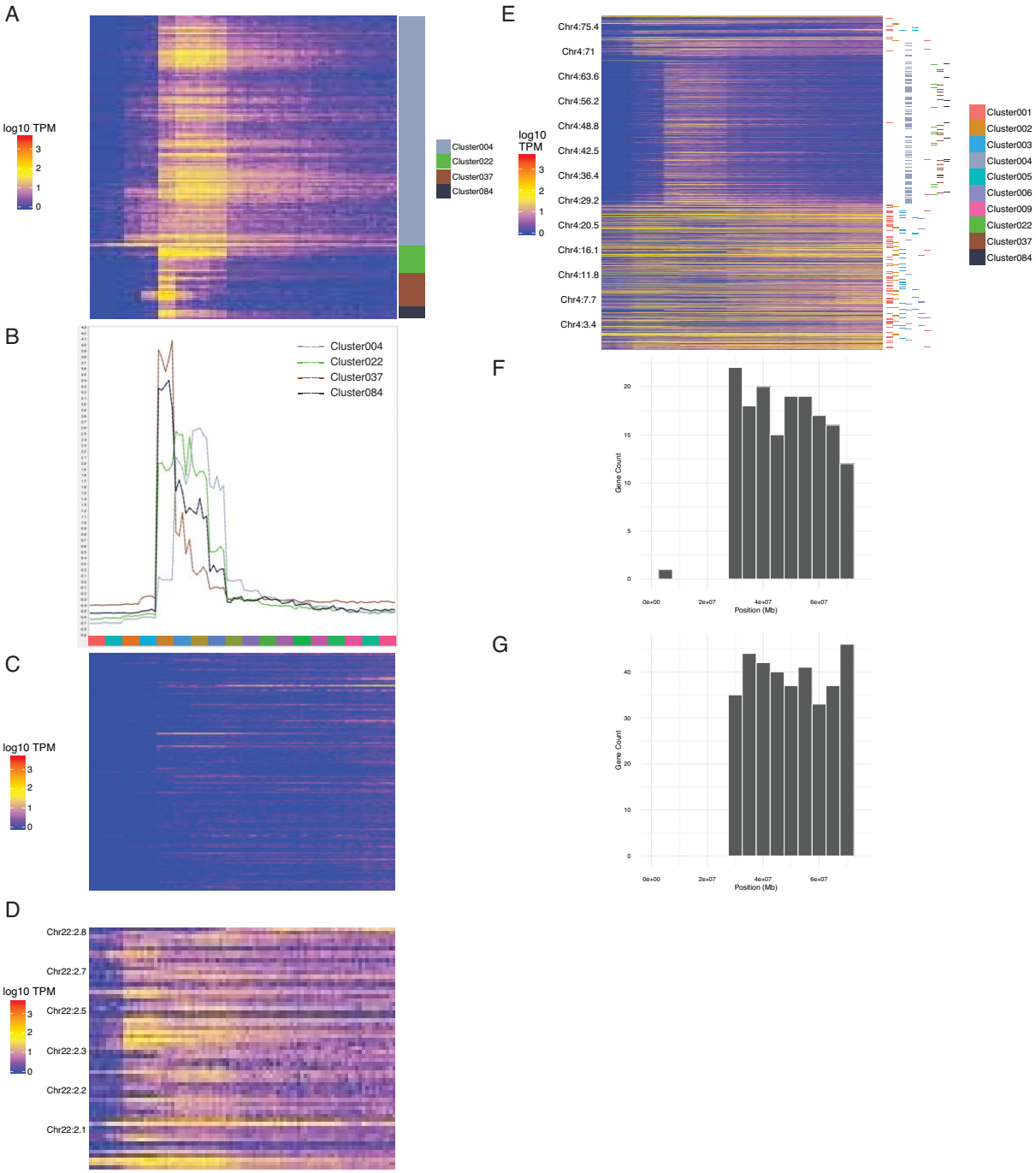

341

342 **Figure 4. ZnF genes expressed at the onset of zygotic transcription.** (A)
343 Heatmap showing the expression profiles (log10 TPM) of the ZnF genes from
344 clusters 4, 22, 37 and 84. (B) Expression profiles of clusters 4, 22, 37 and 84 shown

as average expression (mean centered and variance scaled). (C) Heatmap showing the expression profiles (log10 TPM) of the NLR genes present in GRCz10. (D) Heatmap showing the expression of a cluster of ZnF genes on chromosome 22 displayed in chromosome order. (E) Heatmap showing the expression of all genes on chromosome 4 (log10 TPM) in chromosomal order with cluster assignments shown on the right. (F-G) Histograms showing the distribution of ZnF (F) and NLR (G) genes on chromosome 4.

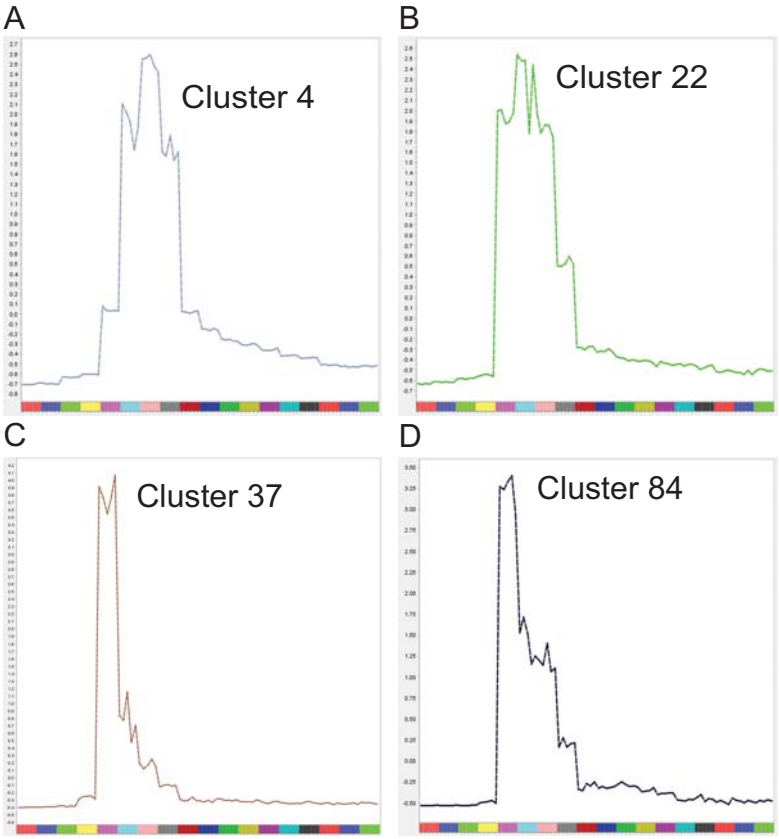

Figure 4-1. BioLayout cluster profiles. Individual expression profiles of clusters 4 (A), 22 (B), 37 (C) and 84 (D) shown as average expression (mean centered and variance scaled).

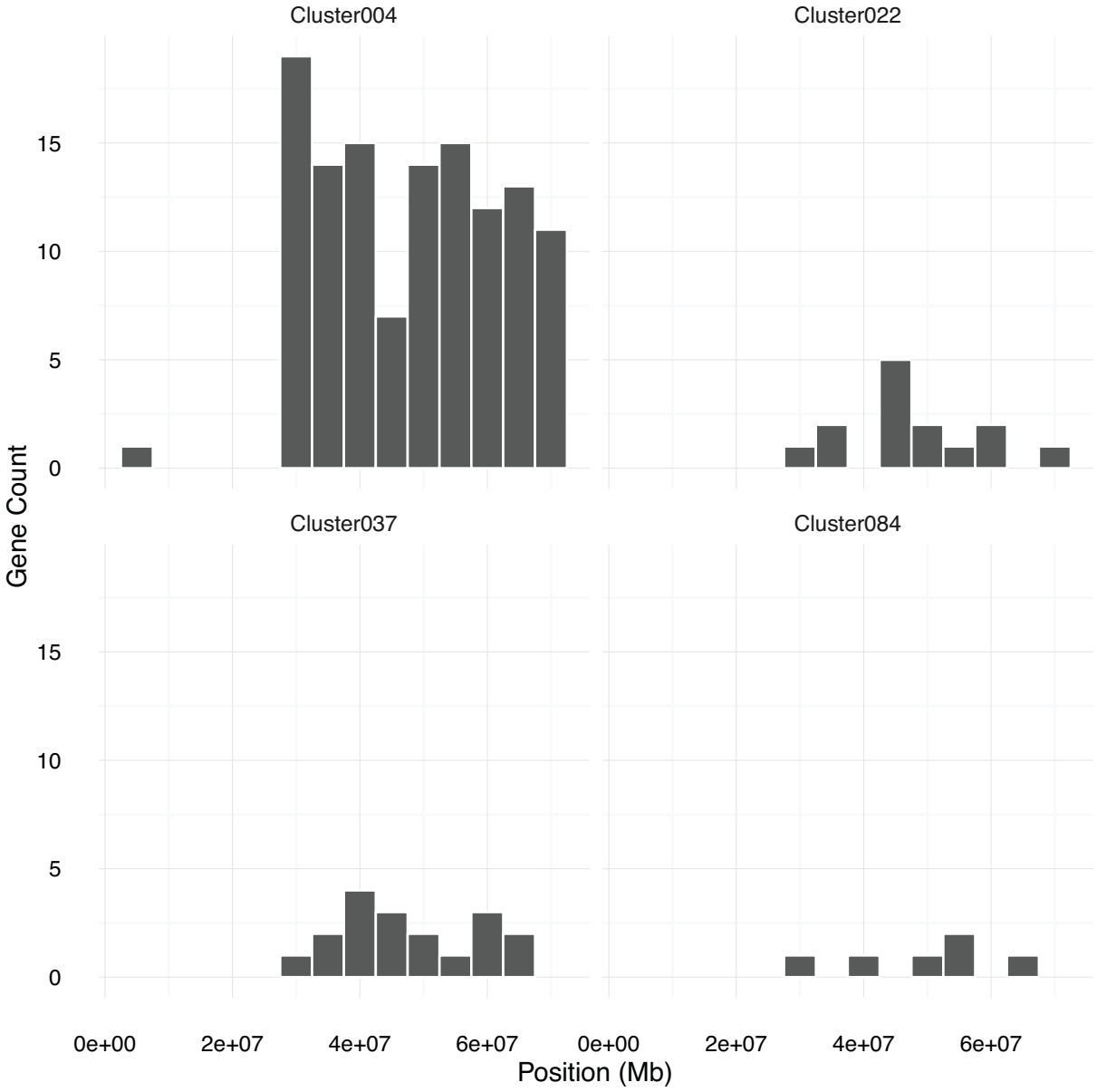

Figure 4-2. Chromosomal distribution of the chromosome 4 ZnF genes. Individual histograms split by cluster showing the chromosomal distribution of the ZnF genes from clusters 4, 22, 37 and 84.

This effect can even be seen on the chromosomal scale. A plot of the expression profiles of all the genes across chromosome 4 in chromosomal order shows a domain on the long arm that is enriched for these ZnF genes (Figure 4E) that share a similar expression pattern.

368 **Table1**

Cluster	Chromosome	Count	Expected	log2FE	Adjusted pvalue
Cluster023	Chr1	9	2.25	2.00	1.161e-02
Cluster004	Chr4	129	47.29	1.45	7.434e-24
Cluster022	Chr4	14	5.03	1.48	1.156e-02
Cluster037	Chr4	23	3.35	2.78	9.033e-14
Cluster084	Chr4	9	1.48	2.61	1.659e-04
Cluster074	Chr12	8	0.48	4.05	6.337e-07

369

370 Table 1. BioLayout clusters with significant chromosomal enrichments (adjusted p-value <
371 0.05 and log2 fold enrichment [log2FE] > 1).

372

373 ## Chromosomal expression domains

374 Since the expression pattern of the chromosome 4 ZnF genes is obvious on a
375 chromosome level plot, we wondered if it was possible to find any other
376 chromosomal regions where the genes share a common expression pattern. To
377 investigate this, we plotted the expression of all the genes for each chromosome in
378 chromosomal order (Supplemental Figure 4-3A). This led to the identification of
379 another region with genes containing zinc finger domains, this time on chromosome
380 22 (Figure 4D). These genes begin to be expressed at a similar stage to the
381 chromosome 4 ZnF genes, although they tend to be more widely expressed over the
382 time course (Figure 4D).

383 There are also several other domains of co-expressed genes that can be clearly
384 seen at the chromosome level, such as the gamma crystallin family of genes on
385 chromosome 9, that are all highly expressed at the end of the time series
386 (Supplemental Figure 4-3B).

387 Interestingly, there is a small region on chromosome 12 where the genes are all
388 expressed from late gastrula through to the end of the pharyngula period

389 (Supplemental Figure 4-3C). The genes in this region all have clone-based names
390 apart from *ctslb* (ENSDARG00000039173, also known as *hatching gland 1*, *hgg1*).
391 All of them appear in the same BioLayout cluster (cluster 74), which has an
392 overrepresentation of genes on chromosome 12 (Table 1). This appears to be a fish-
393 specific expansion of cathepsin L. Similar expansions have happened in multiple
394 different lineages including rodents
395 (http://www.ensembl.org/Mus_musculus/Gene/SpeciesTree?db=core;g=ENSMUSG0
396 0000021477;r=13:64363214-64370306;t=ENSMUST00000021933).
397 On chromosome 11 there is a cluster containing hairy and enhancer of split-related
398 genes and a set of unnamed genes all expressed from late gastrula through
399 segmentation and pharyngula stages (Supplemental Figure 4-3D). Finally, two
400 clusters of genes containing histone domains can be seen on chromosomes 7 and
401 25 (Supplemental Figure 4-3E-G).

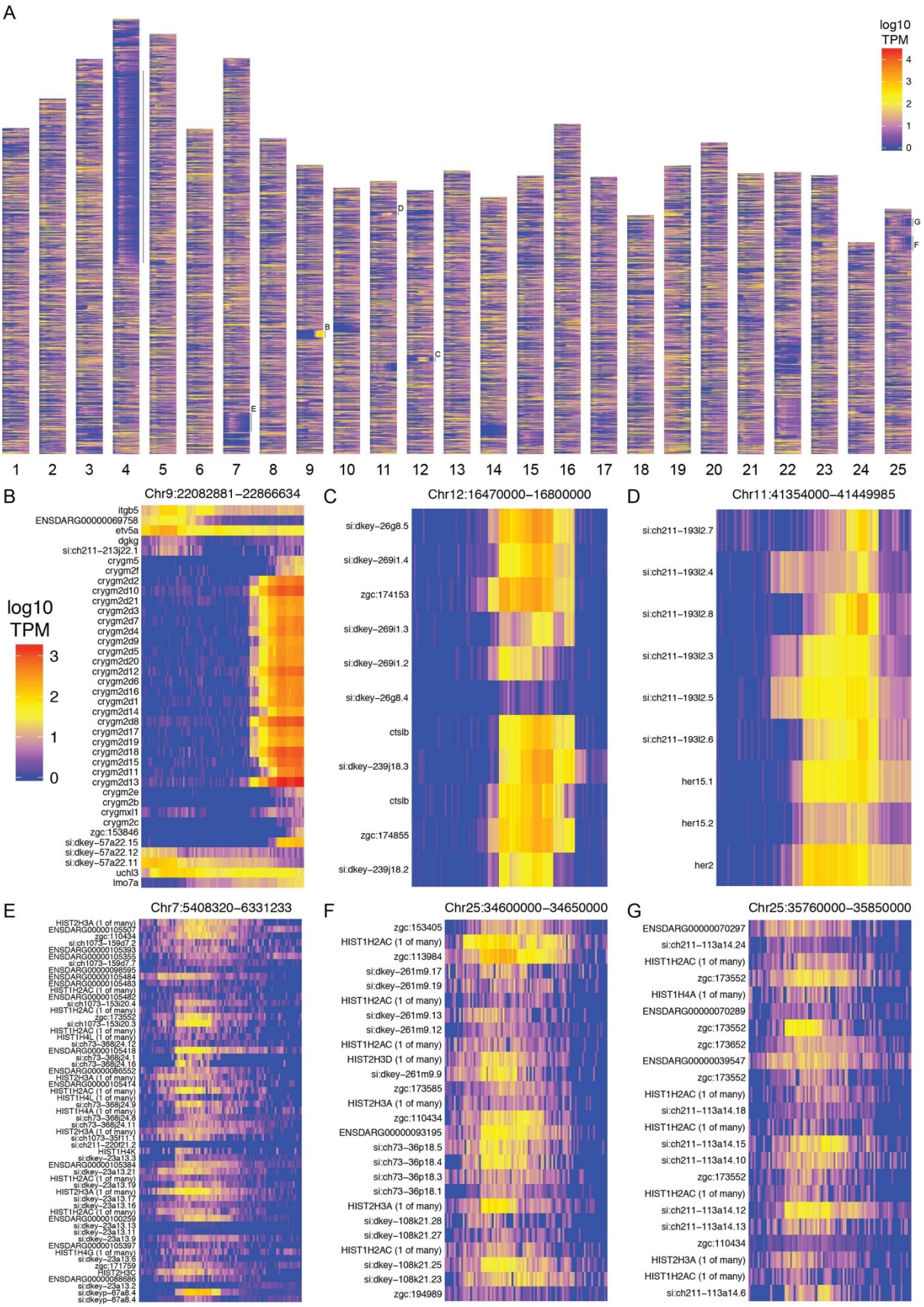

Figure 4-3. Chromosomal expression domains. (A) Heatmaps showing the expression profiles (log10 TPM) of genes in chromosomal order. The unlabelled line

405 next to chromosome 4 marks the location of the ZnF genes shown in Figure 4. (B-G)
406 Expression profile heatmaps of the regions indicated by letters in (A).

407 Conservation/Divergence of the expression profiles of
408 paralogous genes

409 Teleost fish underwent a third round of whole genome duplication compared to the
410 two rounds of tetrapods. During rediploidisation, most of the duplicate genes were
411 lost, however a significant proportion were retained and are now present as
412 paralogous pairs. Paralogous genes can have conserved expression patterns but
413 often the expression patterns have diverged so that the paralogues function at
414 different times or in different tissues. To investigate whether we can see this in our
415 data, which has only stage and not tissue specificity information, we produced a list
416 of one-to-one teleost-specific paralogues pairs using data from Ensembl (3144 gene
417 pairs with expression in our data).

418 We calculated the Pearson correlation coefficients between the normalised counts
419 for each paralogous pair as a measure of how similar the expression profiles are. A
420 histogram of the correlation coefficients shows a distribution skewed to high positive
421 correlations (Figure 5A) when compared to a random sample of gene pairs of similar
422 size (Figure 5B). Despite this skew, there is a significant proportion of the distribution
423 with low or negative correlation coefficients, suggesting that this may represent a set
424 of genes whose expression patterns have diverged (50% of the distribution is below
425 0.45).

426 Examples of highly correlated and negatively correlated genes are shown in Figure
427 5C-G and Supplemental Figure 5-1. To get an estimate of how many of these gene
428 pairs have divergent spatial expression patterns, we used the ZFA annotation
429 provided by ZFIN. There are 683 gene pairs where there is anatomical expression
430 information for both genes. For each pair we counted up the intersection of all the
431 pairs of stage ID and anatomy term that make up the expression annotations. For
432 the pairs studied, 83.7% (572 pairs) have an intersection of less than 50%.

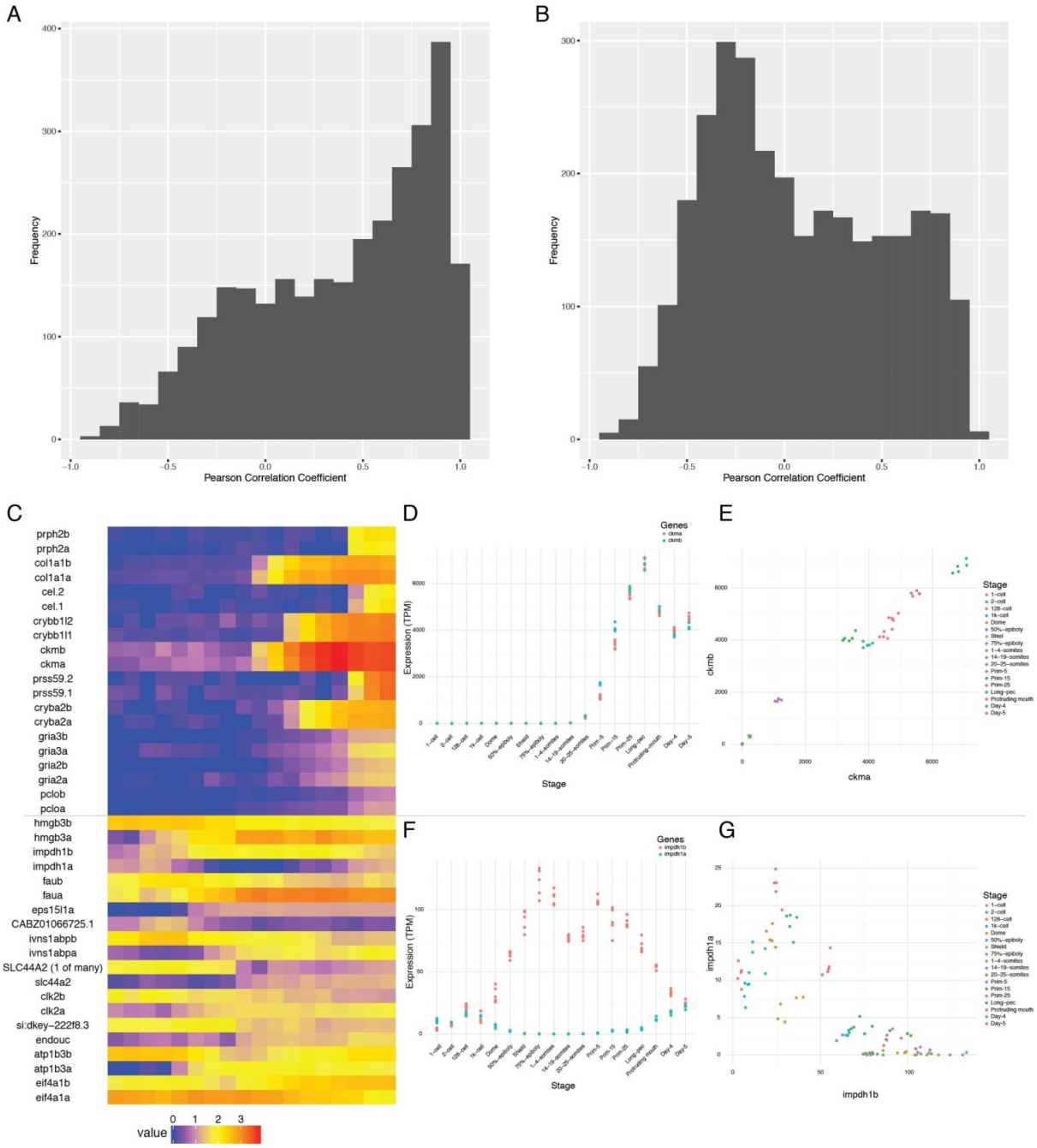

Figure 5. Conservation/divergence of paralogous genes. (A-B) Histograms of Pearson correlation coefficients among one-to-one paralogous gene pairs (A) and a random sample of genes (B). (C) Heatmap showing the expression of the gene pairs with the top 10 highest correlation coefficients (top half) and the top 10 most negative correlation coefficients (bottom half). (D-E) Plots showing the expression of *ckma/b* by stage (D) and plotted against each other (E). (F-G) Plots showing the expression of *impdh1a/b* by stage (F) and plotted against each other (G).

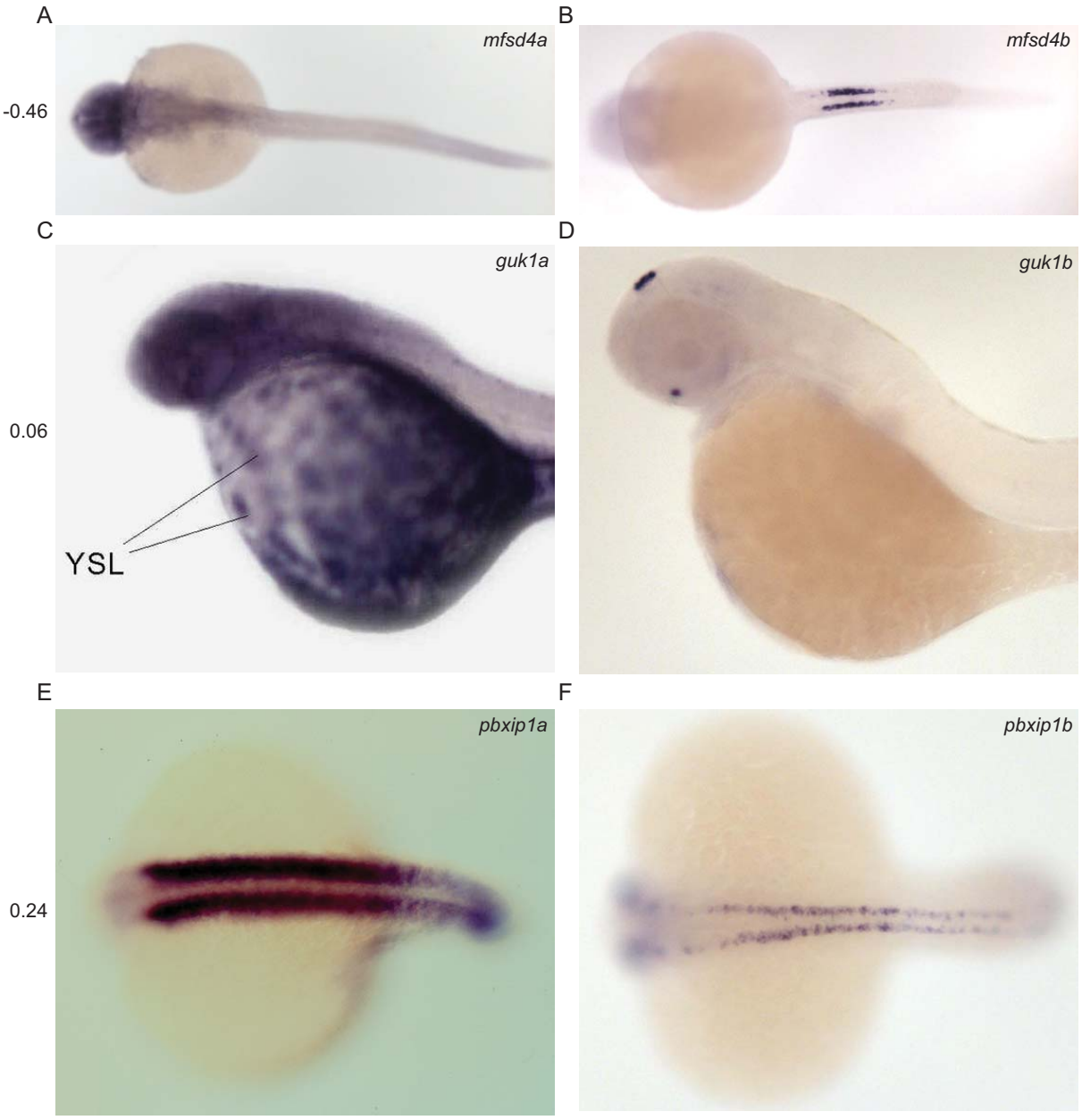

Figure 5-1. Divergent expression of paralogous pairs. Images from ZFIN (ZFIN.org) showing examples of paralogous gene pairs with diverged expression patterns. The Pearson correlation coefficient between the RNA-seq expression profiles of each pair is shown to the left. (A-B) *mfsd4a/b*. (C-D) *guk1a/b*. (E-F) *pbxip1a/b*.

Alternative 3′ end use

To catalogue alternative 3′ end usage across development we produced 3′ pulldown data for the same time points as the RNA-seq. There are multiple possible consequences of alternative 3′ ends, such as different/extra 3′ UTR sequence

452 (Figure 6A). This could provide different binding sites for RNA-binding proteins or
453 regulation by microRNAs. For example, one transcript may contain a microRNA
454 binding site lacking in another, changing post-transcriptional regulation. Other
455 possibilities include different/extra coding sequence at the 3′ end of transcripts,
456 leading to proteins that contain different domains and therefore different molecular
457 functions.

458 Across all 423 samples over all the stages, there were 253,627 regions identified,
459 where each region may be associated with multiple 3′ ends. However, many of these
460 are false positives due to poly(T) pulldown from genomic poly(A) tracts within
461 transcripts. These regions are then filtered by various criteria such as distance to an
462 annotated gene and genomic context in an attempt to remove artefactual regions
463 (Figure 6B and Methods), which reduces the set to 37,724 regions. For this analysis,
464 we increased the stringency of filtering to reduce the inclusion of false-positive ends
465 and produce a high-confidence set of 3′ ends to work from. This stricter set contains
466 8358 regions. Once the regions have been associated with annotated genes, 1551
467 genes have two or more 3′ ends.

468 This high-confidence set has allowed us to define 3′ ends of genes that are
469 alternatively used throughout development. For example, *pdlim5b*
470 (ENSDARG00000027600) has three alternative 3′ ends which are used at different
471 times during development (Figure 6C-E). During cleavage and gastrula stages, one
472 particular end is used (end 2 in Figure 6C), but all three are observed during
473 segmentation stages. Ends 1 and 2 would be predicted to produce the same protein
474 with different 3′ UTRs, allowing for differential post-transcriptional regulation.
475 However, end 3 is predicted to produce a protein which lacks the C-terminal zinc
476 finger domain, allowing for this alternative transcript to have a completely different
477 molecular function.

478

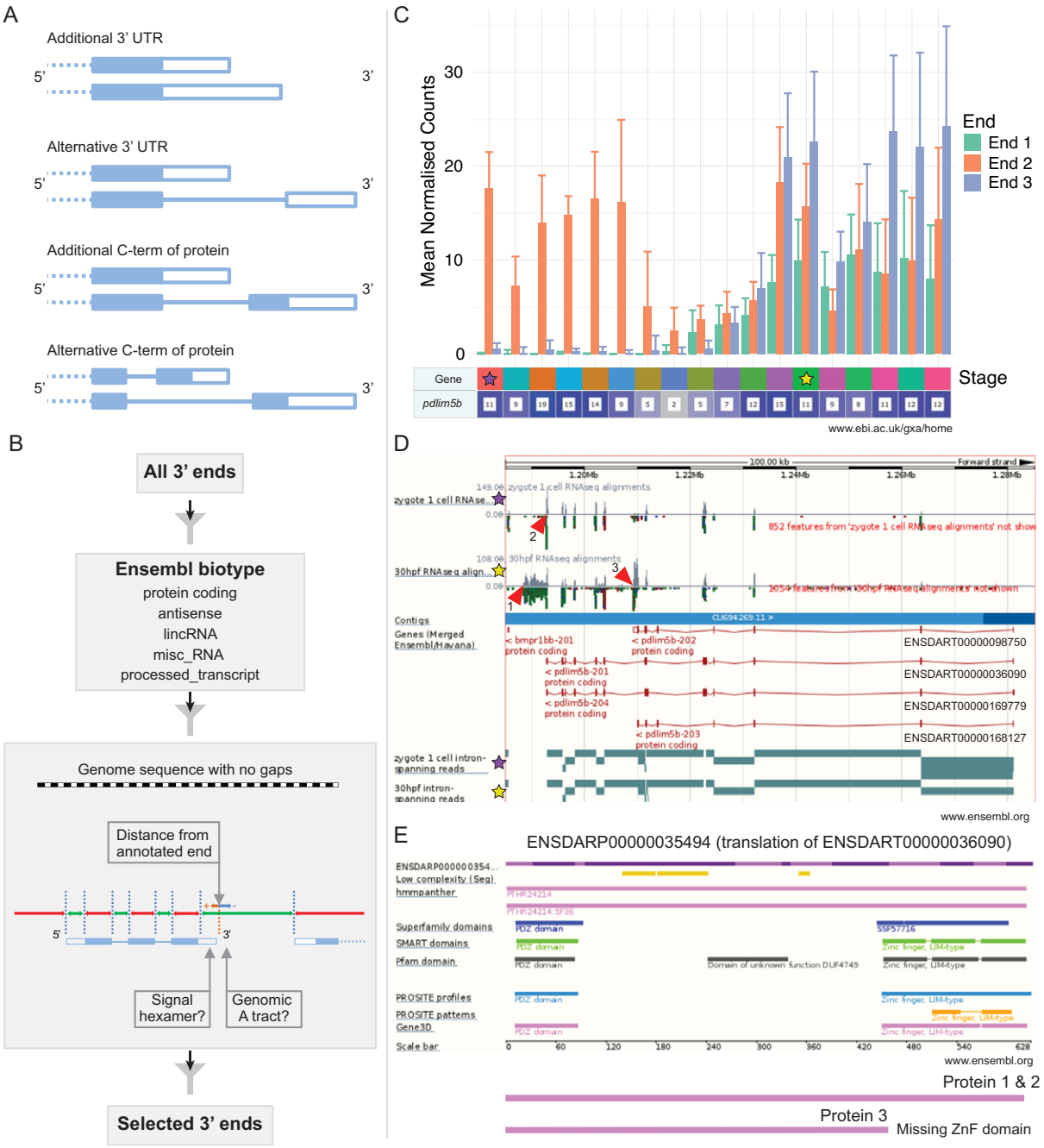

Figure 6. Alternative 3' end use during development. (A) Diagrams showing the alternative possible outcomes of differential 3' end usage. Only the 3' end of the gene is shown where the exons are boxes, the introns are represented as lines and filled boxes are coding. The dotted line represents the remaining 5' end of the gene. (B) Flowchart showing the DeTCT 3' end filtering strategy. (C) Graph showing the mean normalised counts by stage for the three alternative 3' ends (shown in D) of the *pdlim5b* gene. Error bars represent standard deviations. Underneath is a screenshot from Expression Atlas (Sept 2016) showing the overall FPKM for

489 *pdlim5b*. The stages for which exon and intron data are shown in D are denoted with
490 stars. (D) Screenshot from Ensembl (release 87) showing the *pdlim5b* gene
491 (10:1185001-1285000). The purple stars mark exon read counts for the 1-cell stage
492 at the top and intron spanning read counts at the bottom. Similarly, prim-15 counts
493 are marked by yellow stars. Red arrowheads point to the genomic positions of the
494 three transcript ends. Note 3' UTR resulting in end 1 is not annotated in this gene
495 build. Four transcripts are labelled on the right hand side. (E) A snapshot of Ensembl
496 release 87 protein view showing *pdlim5b* transcript ENSDART00000036090.6 from
497 N-terminus to C-terminus. The protein domains missing if the transcript finished at
498 end 3 are shown below.

499 Novel primary miRNA transcripts

500 Along with cataloguing 3′ ends, we have performed RNA-seq on mutants for two
501 genes involved in microRNA (miRNA) maturation, in order to annotate the
502 polyadenylated primary miRNA transcripts. Mature miRNAs are released from longer
503 primary transcripts (pri-miRNAs) by a series of processing steps (Denli et al., 2004;
504 Gregory et al., 2004; Grishok et al., 2001; Hutvagner et al., 2001). First, precursor
505 hairpins (pre-miRNAs) are sliced from the host transcript in the nucleus by the
506 microprocessor complex, consisting of the proteins Drosha (Rnasen) and Dgcr8
507 (Pasha). Subsequently the hairpin is cut by Dicer1 in the cytoplasm, freeing the
508 miRNA duplex.

509 Although much effort has been dedicated to sequencing and annotating the mature
510 miRNAs themselves, the annotation of many primary miRNA genes is likely hindered
511 by their rapid nuclear processing. Reasoning that the depletion of *drosha* and *dgcr8*
512 may enrich the transcriptome for unprocessed pri-miRNAs (Chang et al., 2015), we
513 sequenced RNA derived from *dgcr8* and *drosha* wild-type, heterozygous and
514 homozygous mutant embryos to determine whether this would allow us to improve
515 the current pri-miRNA annotation. Following the assembly of the transcriptome, we
516 were able to better define a large number of novel pri-miRNA loci not annotated in
517 the current Ensembl release (v87) (Fig. 7). The v87 release includes 313 pri-miRNA
518 transcripts overlapping 220 annotated miRNA loci. Our assembly contains 398 pri-
519 miRNA transcripts which overlap 283 miRNA loci, 94 of which are not currently
520 associated with a pri-miRNA (Figure 7D, Supplemental Data File 11 & 12). These will

521 be incorporated into a future Ensembl gene set update.

522

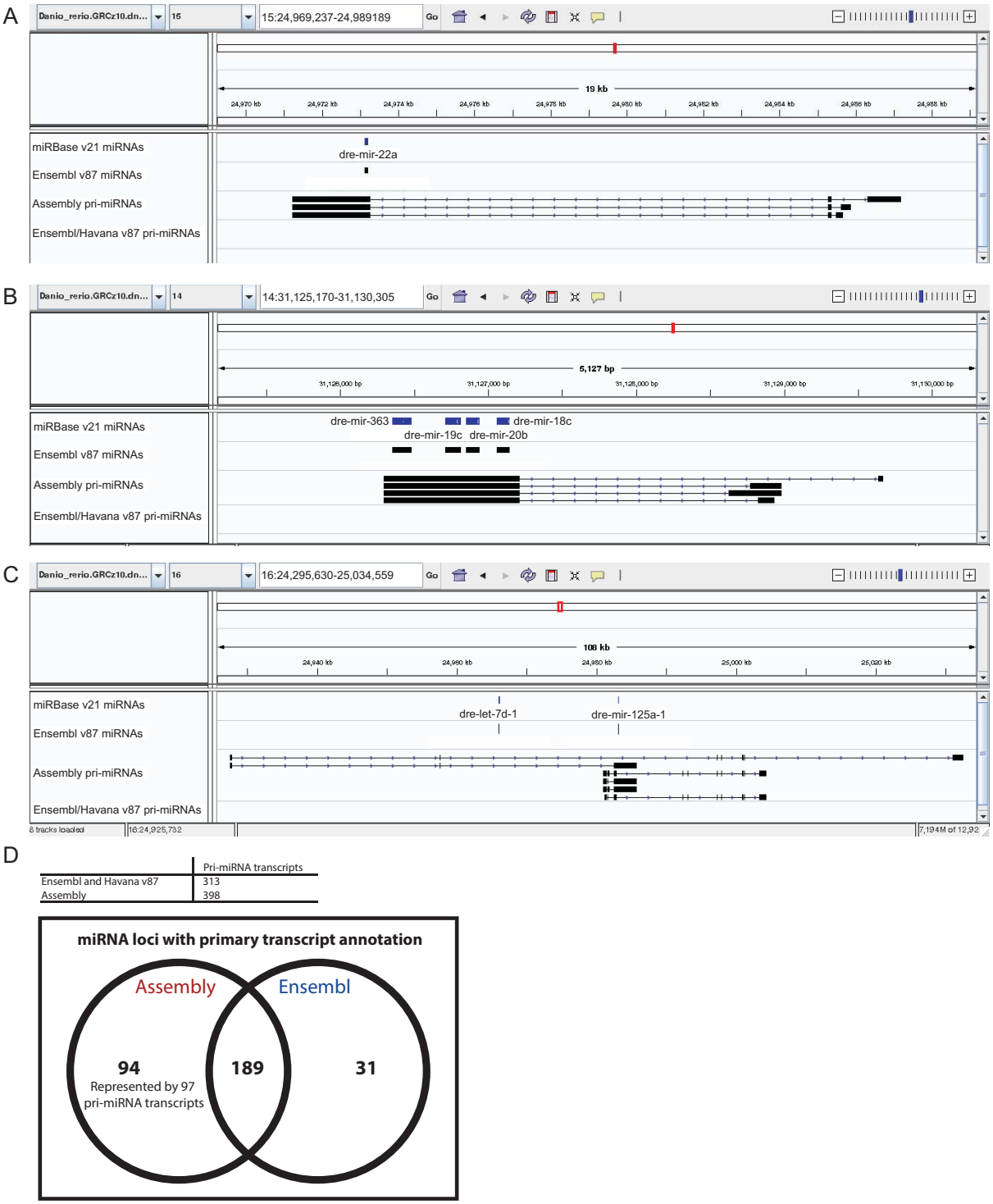

	Pri-miRNA transcripts
Ensembl and Havana v87	313
Assembly	398

523

524 **Figure 7. Annotation of primary miRNA transcripts.** (A-C) A selection of miRNA
525 loci for which pri-miRNA annotation is not available in Ensembl and Havana v87. IGV
526 screen shots showing pri-miRNA transcripts overlapping mir-22a (A), mir-363, mir-
527 19c, mir-20b and mir-18c (B), and mir-125 (C). Tracks shown are miRNA

528 annotations from miRBase and Ensembl, newly assembled pri-miRNA transcripts
529 and Ensembl pri-miRNAs. (D) Table and Venn diagram showing the numbers of
530 assembled pri-miRNA transcripts and the overlap with of Ensembl miRNAs with an
531 annotated pri-miRNA.

532 Discussion

533 We have produced a high quality map of zebrafish mRNA expression during
534 development. It represents the first detailed temporal mRNA reference in zebrafish
535 and enhances our understanding of the transcriptional diversity underlying vertebrate
536 development.

537 Ordering the gene set by the stage at which they have their maximum expression
538 gives a detailed overview of development, showing the molecular correlates of
539 morphological changes within the embryo. This arrangement of the dataset reveals
540 that there is a much larger fraction of unnamed genes in the stages from dome to
541 75% epiboly. We find that this peak in unnamed genes during gastrulation is not
542 driven by an enrichment for teleost or zebrafish-specific genes, as the proportion of
543 unnamed genes with mammalian orthologues is at the same level during these
544 stages as during the rest of development. This implies that there is a large number of
545 genes involved in vertebrate gastrulation that have yet to be characterised.

546 Having a large number of stages and replicates allows us to cluster genes by their
547 expression profile across all of development using a graph-based method. This splits
548 the assayed genes into 252 different expression profiles containing at least 5 genes
549 each (10,363 of the genes are assigned to clusters). GO/ZFA enrichment on these
550 clusters allows us to associate unnamed genes with known processes.

551 One intriguing set of clusters contains an over-representation of genes on the long
552 arm of chromosome 4, a region considered to be constitutive heterochromatin (Howe
553 et al., 2013b). The vast majority of these genes encode proteins with zinc finger
554 domains. The clusters show expression profiles that rise sharply around the time of
555 zygotic genome activation (ZGA) and decrease at the latest after 75% epiboly. Given
556 this, it is tempting to speculate that these genes have a role during the activation of
557 the zygotic genome. In *Drosophila* the zinc finger gene Zelda (zld) is involved in
558 zygotic genome activation by early and widespread binding to promoters and

559 enhancers ahead of their genes' activation during the maternal-zygotic transition
560 (Harrison et al., 2010; Harrison et al., 2011; Liang et al., 2008). In zebrafish, *pou5f3*,
561 *nanog* and *soxB* genes have been implicated in activating specific genes during ZGA
562 (Lee et al., 2013; Leichsenring et al., 2013), but no general factor comparable to
563 Zelda has been identified yet. It is possible that the role of the ZnF protein family
564 genes on chromosome 4 is to set up or maintain open chromatin in a genome-wide
565 way to allow for the rapid activation of the first zygotic genes. This is supported by
566 the finding that these clusters also contain four unnamed genes, also found on
567 chromosome 4, that are predicted to be H3K36 methyltransferases
568 (ENSDARG00000104681, ENSDARG00000091062, ENSDARG00000076160,
569 ENSDARG00000103283). H3K36 methylation is generally, albeit not exclusively,
570 associated with active euchromatin (Wagner and Carpenter, 2012). Another option is
571 that they could be responsible for negatively regulating areas of open chromatin to
572 stop inappropriate activation of transposable elements during ZGA. In mammals,
573 suppression of retrotransposons is mediated by the rapidly evolving KRAB zinc
574 finger genes (Jacobs et al., 2014). KRAB zinc finger genes are exclusive to
575 mammals, making the chromosome 4 ZnF genes a possible functional equivalent.
576 Also, as would be expected given their expression profiles, within these four clusters
577 are a large number of well-known developmental regulators such as members of the
578 Tgf-beta (Bmp and Nodal) and Wnt signalling pathways, as well as transcription
579 factors such as *gata5* & *6*, *sox32*, *vox*, *ved*, *vent* and both *Brachyury* homologues.
580 Correlation analysis of paralogues stemming from a teleost-specific genome
581 duplication shows that while there is the expected skew towards positive temporal
582 expression correlation, a significant proportion of paralogues have diverged in their
583 expression pattern as demonstrated by low or negative correlation coefficients. This
584 is confirmed by an analysis of the expression annotations provided by ZFIN. There
585 are caveats to this analysis, not least that the annotation is far from complete and,
586 therefore, annotations may not overlap simply because a certain stage has been
587 investigated for one paralogue, but not the other. It will also be the case that some
588 genes have expression patterns that are diverged spatially, but not temporally. Thus
589 the number of genes whose expression annotations do not overlap is an estimate,
590 but it does suggest that the phenomenon of divergence is widespread among

591 paralogues, something that might be expected to be the case since there needs to
592 be some form of selective pressure on retaining paralogous pairs.

593 A further layer of complexity is added by differential exon and 3′ end use. The
594 dataset uncovers new splice isoforms which, when viewed in Ensembl against the
595 Ensembl genebuild, will refines the current gene annotation and ties splice isoforms
596 to their temporal expression patterns. This is of particular relevance to the ongoing
597 debate surrounding reverse genetics approaches in zebrafish (Kok et al., 2015). One
598 possible explanation for phenotypic discrepancies between morpholino antisense
599 oligo knockdown, code disrupting point mutations and CRISPR/Cas9 or TALEN-
600 mediated larger deletions is that mutations affect potentially non-critical exons that
601 are only present in a subset of transcripts of a given gene. An improved annotation
602 that gives temporal resolution of exon usage will be of tremendous value for the
603 identification of critical exons.

604 Using the 3′ end sequencing method DeTCT, we have catalogued the differential
605 use of alternative 3′ ends in a filtered set of transcripts. In accordance with previous
606 work on a subset of stages (Collins et al., 2012; Sheppard et al., 2013; Ulitsky et al.,
607 2012) we find that there is differential use of not only 3′ UTRs but also coding
608 sequence across development. We show that *pdlim5b* is expressed as several
609 transcripts, with a single maternal isoform and multiple zygotic ones producing
610 different proteins. Incorporation of the data into an updated gene set will
611 systematically identify these and refines our understanding of gene regulation.
612 Furthermore, it provides scope for temporally resolved analysis using transcript-
613 specific knockout targeting strategies.

614 An important role of 3′ UTRs is in post-transcriptional regulation of their transcripts.
615 The 3′ UTRs contain binding sites for miRNAs which silence transcripts through
616 translational repression or mRNA destabilisation (Bartel, 2009). However, the
617 primary transcripts of miRNAs are often poorly annotated. Using two miRNA
618 processing mutants (*dgcr8* and *drosha*), we have produced an improved pri-miRNA
619 assembly with an increase of 42% in the number of Ensembl miRNAs with an
620 associated primary transcript. In agreement with previous studies (Chang et al.,
621 2015; Gaeta et al., 2017), the assembly shows that miRNAs are processed from
622 primary transcripts with multiple isoforms with potentially multiple transcription start
623 sites (Figure 7). This diversity of transcripts means that the expression of miRNAs in

relatively close proximity (e.g. dre-let-7d-1 and dre-mir-125a-1) could be regulated at multiple levels (Figure 7C). In some transcripts both let-7d-1 and mir-125a-1 are both intronic and in some mir-125a-1 is exonic. There are also transcripts with alternate promoters which exclude the let-7d-1 locus entirely. These features provide significant flexibility to the transcriptional regulation of miRNAs. It is possible that a proportion of the assembled constructs are fragments. Clear definition of the 5' and 3' termini will require further work and ultimately experimental validation by an alternative method such as 5′ rapid amplification of cDNA ends.

A major aim for this work was to create an accessible reference of normal mRNA expression during zebrafish development. The primary sequence is available from the European Nucleotide Archive (ENA, http://www.ebi.ac.uk/ena), but importantly has also been interpreted for immediate user-friendly access. Expression Atlas provides relative expression levels while Ensembl displays alternative genomic transcript structures alongside the current gene annotation. These pre-computed analyses allow an in-depth examination of the data on a gene by gene basis. This makes it easy for researchers to benefit from the data and provides a direct link to the wealth of information present in genomic databases.

Materials and Methods

Animal Care

Zebrafish were maintained in accordance with UK Home Office regulations, UK Animals (Scientific Procedures) Act 1986, under project licence 70/7606, which was reviewed by the Wellcome Trust Sanger Institute Ethical Review Committee.

Sample collection

Wild-type HLF strain zebrafish (*Danio rerio*) were maintained at 28.5 °C on a 14h light/10h dark cycle. At the time of mating, breeding males and females were separated overnight before letting them spawn naturally in the morning to allow for synchronisation of developmental stages. Fertilised eggs were grown at 28°C and staged using previously defined criteria (Kimmel et al., 1995). Samples from 18 different developmental stages from 1-cell to 5 days post fertilisation were collected

653 by snap freezing the embryos in dry ice. Details of sample names and accession
654 numbers are provided in Supplemental Data File 1.

655 RNA Extraction

656 RNA was extracted from embryos by mechanical lysis in RLT buffer (Qiagen)
657 containing 1 µl of 14.3M beta mercaptoethanol (Sigma). The lysate was combined
658 with 1.8 volumes of Agencourt RNAClean XP (Beckman Coulter) beads and allowed
659 to bind for 10 minutes. The plate was applied to a plate magnet (Invitrogen) until the
660 solution cleared and the supernatant was removed without disturbing the beads. This
661 was followed by washing the beads three times with 70% ethanol. After the last
662 wash, the pellet was allowed to air dry for 10 mins and then resuspended in 50 µl of
663 RNAse-free water. RNA was eluted from the beads by applying the plate to the
664 magnetic rack. RNA was quantified using Quant-IT RNA assay (Invitrogen) for
665 samples 24 hours post-fertilisation and older.

666 RNA Sequencing

667 Total RNA from 12 embryos was pooled and DNase treated for 20 mins at 37°C
668 followed by addition of 1 µl 0.5M EDTA and inactivation at 75°C for 10 mins to
669 remove residual DNA. RNA was then cleaned using 2 volumes of Agencourt
670 RNAClean XP (Beckman Coulter) beads under the standard protocol. Five replicate
671 libraries were made for each stage using 700 ng total RNA and ERCC spike mix 2
672 (Ambion). Strand-specific RNA-seq libraries containing unique index sequences in
673 the adapter were generated simultaneously following the dUTP method. Libraries
674 were pooled and sequenced on Illumina HiSeq 2500 in 100bp paired-end mode.
675 Sequence data were deposited in ENA under accession ERP014517.

676 FASTQ files were aligned to the GRCz10 reference genome using tophat (v2.0.13,
677 options: --library-type fr-firststrand). Counts for genes were produced using htseq-
678 count (v0.6.0 options: --stranded=reverse) with the Ensembl v85 annotation as a
679 reference. The processed count data are in Supplemental Data File 2.

680 # DeTCT

681 DeTCT libraries were generated, sequenced and analysed as described previously
682 (Collins et al., 2015). The resulting genomic regions and putative 3′ ends were
683 filtered stringently using DeTCT's filter_output script
684 (https://github.com/iansealy/DETCT/blob/master/script/filter_output.pl) in its --stricter
685 mode. This mode removes 3′ ends more than 5000 bases downstream of existing
686 protein-coding annotation (Ensembl v86) or more than 50 bases from existing non-
687 coding annotation (antisense, lincRNA, misc_RNA and processed_transcript
688 biotypes). 3′ ends are also removed if nearby sequence is enriched for As, if within
689 14 bp of an N, if within a simple repeat (repeats annotated by dust or trf) or a
690 transposon, or if not nearby a primary hexamer. Regions not associated with 3′ ends
691 are also removed. Sequence data were deposited in ENA under accessions
692 ERP006948 and ERP013756. The processed count data is available to download at
693 https://doi.org/10.6084/m9.figshare.4622311.

694 # Analysis

695 ## ZFA enrichment

696 ZFA enrichment was done using Ontologizer (http://ontologizer.de). The ZFA
697 ontology was download from http://www.berkeleybop.org/ontologies/zfa.obo and
698 mappings between ZFIN gene IDs and ZFA IDs was downloaded from ZFIN
699 (http://zfin.org/downloads/wildtype-expression_fish.txt and
700 http://zfin.org/downloads/phenoGeneCleanData_fish.txt). Pvalues were adjusted for
701 testing of both multiple terms and multiple clusters using the Bonferroni correction.

702 ## GO enrichment

703 GO enrichment was done using the R topGO package (Alexa and Rahnenfuhrer,
704 2016). The mapping between Ensembl IDs and GO terms was retrieved from the
705 Ensembl database using a custom perl script (get_ensembl_go_terms.pl) from the
706 topgo-wrapper repository (https://github.com/iansealy/topgo-wrapper).

707

708 **Plots**

709 The code to reproduce all the plots in this paper can be downloaded at github
710 (https://github.com/richysix/zfs-devstages).

711 **BioLayout**

712 BioLayout *Express*^{3D} is available to download for free
713 (http://www.biolayout.org/downloads/). The input expression file is provided as
714 Supplemental Data File 6. The processed layout file of the network displayed in
715 Figure 3B is available at https://doi.org/10.6084/m9.figshare.4622293.

716 pri-miRNA assembly

717 For each mutant allele – sa191, *drosha* (*rnasen*); sa223, *dgcr8* (*pasha*) – we
718 produced and sequenced stranded RNA-seq libraries from homozygous,
719 heterozygous and wild-type embryos (5 replicates of each). Sequence data were
720 deposited in ENA under accession ERP013690. To identify new pri-miRNAs, FASTQ
721 files were aligned to the zebrafish genome (GRCz10) using STAR (v2.5.1a, options:
722 --alignSJoverhangMin 8 --alignSJDBoverhangMin 1 --outFilterMismatchNmax 999 --
723 alignIntronMin 20 --alignIntronMax 1000000 --alignMatesGapMax 1000000 --
724 readFilesCommand zcat --outFilterIntronMotifs RemoveNoncanonical --outFilterType
725 BySJout --outFilterMultimapNmax 10 --sjdbOverhang 74). Ensembl v86 zebrafish
726 annotation was provided as a junction file. Aligned reads were sorted, indexed and
727 mate pairings were fixed using Samtools (v1.3.1). Duplicate alignments were
728 removed with Picard (v2.7.1) (REMOVE_DUPLICATES=true
729 READ_NAME_REGEX=null). Alignments for the homozygous, heterozygous and
730 wild-type samples for both the *drosha* and *dgcr8* lines were merged into two line-
731 specific datasets with Samtools. Each set of merged alignments was then used to
732 assemble a transcriptome with Cufflinks (v2.2.1) (--library-type=fr-firststrand).
733 Ensembl (v86) annotation stripped of rows corresponding to ‘gene’ features was
734 provided as a backbone for the assembly. The *drosha* and *dgcr8* assemblies were
735 then merged with Cuffmerge.

736 Ensembl miRNA annotation (v87) (“miRNA” biotype) was used to define miRNA loci.
737 For the purpose of this analysis we defined pri-miRNAs as any spliced transcript

overlapping at least one of these loci. Ensembl and Havana (v87) annotation was selected as the baseline for novel pri-miRNA prediction. UCSC utilities gtfToGenePred and genePredToBed were used to convert from GTF to BED format. Pri-miRNAs were identified by removing single exon transcripts from the merged assembly and Ensembl annotations and comparing the remainder to annotated miRNA loci using bedtools (v2.24.0) intersect (-wa –s). Finally, assembled pri-miRNA transcripts were filtered to remove those for which either the first or last exon was less than 20nt in length, those which contain an intron greater than 100,000nt, or those which contain an intron that isn't flanked by the GT-AG or GC-AG motifs (Breathnach et al., 1978).

Acknowledgements

This work was funded by the Wellcome Trust Sanger Institute (grant number WT098051). M. Davis was funded by a MRC Methodology Research Fellowship (MR/L012367/1). Ensembl, Expression Atlas and A. Enright are funded by EMBL core funding. We would like to thank the Wellcome Trust Sanger Institute sequencing pipelines for performing sequencing and the staff of the Research Support Facility for zebrafish care. We also thank Samantha Carruthers, Catherine Scahill and Nicole Staudt for critical reading of the manuscript.

Supplemental Data Files:

Supplemental Data File 1 – Sample Information (.tsv)
Supplemental Data File 2 – RNA-seq count data (.tsv)
Supplemental Data File 3 – Max stage cluster assignments (.tsv)
Supplemental Data File 4 – Max stage cluster ZFA enrichment (.tsv)
Supplemental Data File 5 – Max stage cluster GO enrichment (.tsv)
Supplemental Data File 6 – BioLayout input file (.expression)
Supplemental Data File 7 – BioLayout cluster information (.tsv)
Supplemental Data File 8 – BioLayout cluster ZFA enrichment (.zip)
Supplemental Data File 9 – BioLayout cluster GO enrichment (.tsv)
Supplemental Data File 10 – Regional expression information (.tsv)
Supplemental Data File 11 – Assembled pri-miRNA transcripts (.bed)
Supplemental Data File 12 – Table of overlap of miRNAs (.xlsx)

Competing Interests

The authors declare they have no competing interests.

References

Aanes, H., Winata, C. L., Lin, C. H., Chen, J. P., Srinivasan, K. G., Lee, S. G., Lim, A. Y., Hajan, H. S., Collas, P., Bourque, G., et al. (2011). Zebrafish mRNA sequencing deciphers novelties in transcriptome dynamics during maternal to zygotic transition. *Genome Res* **21**, 1328-1338. doi: 10.1101/gr.116012.110.

Alexa, A. and Rahnenfuhrer, J. (2016). topGO: Enrichment Analysis for Gene Ontology. R package version 2.24.0. doi: https://bioconductor.org/packages/release/bioc/html/topGO.html.

Amsterdam, A., Burgess, S., Golling, G., Chen, W., Sun, Z., Townsend, K., Farrington, S., Haldi, M. and Hopkins, N. (1999). A large-scale insertional mutagenesis screen in zebrafish. *Genes Dev* **13**, 2713-2724. doi:

Bartel, D. P. (2009). MicroRNAs: target recognition and regulatory functions. *Cell* **136**, 215-233. doi: 10.1016/j.cell.2009.01.002.

Behrndt, M., Salbreux, G., Campinho, P., Hauschild, R., Oswald, F., Roensch, J., Grill, S. W. and Heisenberg, C. P. (2012). Forces driving epithelial spreading in zebrafish gastrulation. *Science* **338**, 257-260. doi: 10.1126/science.1224143.

Bertrand, J. Y., Chi, N. C., Santoso, B., Teng, S., Stainier, D. Y. and Traver, D. (2010). Haematopoietic stem cells derive directly from aortic endothelium during development. *Nature* **464**, 108-111. doi: 10.1038/nature08738.

Boeck, M. E., Huynh, C., Gevirtzman, L., Thompson, O. A., Wang, G., Kasper, D. M., Reinke, V., Hillier, L. W. and Waterston, R. H. (2016). The time-resolved transcriptome of C. elegans. *Genome Res* **26**, 1441-1450. doi: 10.1101/gr.202663.115.

Breathnach, R., Benoist, C., O'Hare, K., Gannon, F. and Chambon, P. (1978). Ovalbumin gene: evidence for a leader sequence in mRNA and DNA sequences at the exon-intron boundaries. *Proc Natl Acad Sci U S A* **75**, 4853-4857. doi:

Brown, J. B., Boley, N., Eisman, R., May, G. E., Stoiber, M. H., Duff, M. O., Booth, B. W., Wen, J., Park, S., Suzuki, A. M., et al. (2014). Diversity and dynamics of the Drosophila transcriptome. *Nature* **512**, 393-399. doi: 10.1038/nature12962.

Chang, T. C., Pertea, M., Lee, S., Salzberg, S. L. and Mendell, J. T. (2015). Genome-wide annotation of microRNA primary transcript structures reveals novel regulatory mechanisms. *Genome Res* **25**, 1401-1409. doi: 10.1101/gr.193607.115.

Collins, J. E., Wali, N., Sealy, I. M., Morris, J. A., White, R. J., Leonard, S. R., Jackson, D. K., Jones, M. C., Smerdon, N. C., Zamora, J., et al. (2015). High-throughput and quantitative genome-wide messenger RNA sequencing for molecular phenotyping. *BMC Genomics* **16**, 578. doi: 10.1186/s12864-015-1788-6.

813 **Collins, J. E., White, S., Searle, S. M. and Stemple, D. L.** (2012). Incorporating
814 RNA-seq data into the zebrafish Ensembl genebuild. *Genome Res* **22**, 2067-
815 2078. doi: 10.1101/gr.137901.112.
816 **Denli, A. M., Tops, B. B., Plasterk, R. H., Ketting, R. F. and Hannon, G. J.** (2004).
817 Processing of primary microRNAs by the Microprocessor complex. *Nature*
818 **432**, 231-235. doi: 10.1038/nature03049.
819 **Driever, W., Solnica-Krezel, L., Schier, A. F., Neuhauss, S. C., Malicki, J.,**
820 **Stemple, D. L., Stainier, D. Y., Zwartkruis, F., Abdelilah, S., Rangini, Z., et**
821 **al.** (1996). A genetic screen for mutations affecting embryogenesis in
822 zebrafish. *Development* **123**, 37-46. doi:
823 **Enright, A. J., Van Dongen, S. and Ouzounis, C. A.** (2002). An efficient algorithm
824 for large-scale detection of protein families. *Nucleic Acids Res* **30**, 1575-1584.
825 doi:
826 **Gaeta, X., Le, L., Lin, Y., Xie, Y. and Lowry, W. E.** (2017). Defining Transcriptional
827 Regulatory Mechanisms for Primary let-7 miRNAs. *PLoS One* **12**, e0169237.
828 doi: 10.1371/journal.pone.0169237.
829 **Gehrig, J., Reischl, M., Kalmar, E., Ferg, M., Hadzhiev, Y., Zaucker, A., Song, C.,**
830 **Schindler, S., Liebel, U. and Muller, F.** (2009). Automated high-throughput
831 mapping of promoter-enhancer interactions in zebrafish embryos. *Nat*
832 *Methods* **6**, 911-916. doi: 10.1038/nmeth.1396.
833 **Gerstein, M. B., Rozowsky, J., Yan, K. K., Wang, D., Cheng, C., Brown, J. B.,**
834 **Davis, C. A., Hillier, L., Sisu, C., Li, J. J., et al.** (2014). Comparative analysis
835 of the transcriptome across distant species. *Nature* **512**, 445-448. doi:
836 10.1038/nature13424.
837 **Graveley, B. R., Brooks, A. N., Carlson, J. W., Duff, M. O., Landolin, J. M., Yang,**
838 **L., Artieri, C. G., van Baren, M. J., Boley, N., Booth, B. W., et al.** (2011).
839 The developmental transcriptome of Drosophila melanogaster. *Nature* **471**,
840 473-479. doi: 10.1038/nature09715.
841 **Gregory, R. I., Yan, K. P., Amuthan, G., Chendrimada, T., Doratotaj, B., Cooch,**
842 **N. and Shiekhattar, R.** (2004). The Microprocessor complex mediates the
843 genesis of microRNAs. *Nature* **432**, 235-240. doi: 10.1038/nature03120.
844 **Grishok, A., Pasquinelli, A. E., Conte, D., Li, N., Parrish, S., Ha, I., Baillie, D. L.,**
845 **Fire, A., Ruvkun, G. and Mello, C. C.** (2001). Genes and mechanisms
846 related to RNA interference regulate expression of the small temporal RNAs
847 that control C. elegans developmental timing. *Cell* **106**, 23-34. doi:
848 **Haberle, V., Li, N., Hadzhiev, Y., Plessy, C., Previti, C., Nepal, C., Gehrig, J.,**
849 **Dong, X., Akalin, A., Suzuki, A. M., et al.** (2014). Two independent
850 transcription initiation codes overlap on vertebrate core promoters. *Nature*
851 **507**, 381-385. doi: 10.1038/nature12974.
852 **Haffter, P., Granato, M., Brand, M., Mullins, M. C., Hammerschmidt, M., Kane, D.**
853 **A., Odenthal, J., van Eeden, F. J., Jiang, Y. J., Heisenberg, C. P., et al.**
854 (1996). The identification of genes with unique and essential functions in the
855 development of the zebrafish, Danio rerio. *Development* **123**, 1-36. doi:
856 **Harrison, M. M., Botchan, M. R. and Cline, T. W.** (2010). Grainyhead and Zelda
857 compete for binding to the promoters of the earliest-expressed Drosophila
858 genes. *Dev Biol* **345**, 248-255. doi: 10.1016/j.ydbio.2010.06.026.
859 **Harrison, M. M., Li, X. Y., Kaplan, T., Botchan, M. R. and Eisen, M. B.** (2011).
860 Zelda binding in the early Drosophila melanogaster embryo marks regions
861 subsequently activated at the maternal-to-zygotic transition. *PLoS Genet* **7**,
862 e1002266. doi: 10.1371/journal.pgen.1002266.

863 **Harvey, S. A., Sealy, I., Kettleborough, R., Fenyes, F., White, R., Stemple, D.**
864 **and Smith, J. C.** (2013). Identification of the zebrafish maternal and paternal
865 transcriptomes. *Development* **140**, 2703-2710. doi: 10.1242/dev.095091.
866 **Hashimshony, T., Feder, M., Levin, M., Hall, B. K. and Yanai, I.** (2015).
867 Spatiotemporal transcriptomics reveals the evolutionary history of the
868 endoderm germ layer. *Nature* **519**, 219-222. doi: 10.1038/nature13996.
869 **Howe, D. G., Bradford, Y. M., Conlin, T., Eagle, A. E., Fashena, D., Frazer, K.,**
870 **Knight, J., Mani, P., Martin, R., Moxon, S. A., et al.** (2013a). ZFIN, the
871 Zebrafish Model Organism Database: increased support for mutants and
872 transgenics. *Nucleic Acids Res* **41**, D854-860. doi: 10.1093/nar/gks938.
873 **Howe, K., Clark, M. D., Torroja, C. F., Torrance, J., Berthelot, C., Muffato, M.,**
874 **Collins, J. E., Humphray, S., McLaren, K., Matthews, L., et al.** (2013b). The
875 zebrafish reference genome sequence and its relationship to the human
876 genome. *Nature* **496**, 498-503. doi: 10.1038/nature12111.
877 **Howe, K., Schiffer, P. H., Zielinski, J., Wiehe, T., Laird, G. K., Marioni, J. C.,**
878 **Soylemez, O., Kondrashov, F. and Leptin, M.** (2016). Structure and
879 evolutionary history of a large family of NLR proteins in the zebrafish. *Open*
880 *Biol* **6**, 160009. doi: 10.1098/rsob.160009.
881 **Hutvagner, G., McLachlan, J., Pasquinelli, A. E., Balint, E., Tuschl, T. and**
882 **Zamore, P. D.** (2001). A cellular function for the RNA-interference enzyme
883 Dicer in the maturation of the let-7 small temporal RNA. *Science* **293**, 834-
884 838. doi: 10.1126/science.1062961.
885 **Jacobs, F. M., Greenberg, D., Nguyen, N., Haeussler, M., Ewing, A. D., Katzman,**
886 **S., Paten, B., Salama, S. R. and Haussler, D.** (2014). An evolutionary arms
887 race between KRAB zinc-finger genes ZNF91/93 and SVA/L1
888 retrotransposons. *Nature* **516**, 242-245. doi: 10.1038/nature13760.
889 **Kaaij, L. J., Mokry, M., Zhou, M., Musheev, M., Geeven, G., Melquiond, A. S., de**
890 **Jesus Domingues, A. M., de Laat, W., Niehrs, C., Smith, A. D., et al.**
891 (2016). Enhancers reside in a unique epigenetic environment during early
892 zebrafish development. *Genome Biol* **17**, 146. doi: 10.1186/s13059-016-1013-
893 1.
894 **Kettleborough, R. N., Busch-Nentwich, E. M., Harvey, S. A., Dooley, C. M., de**
895 **Bruijn, E., van Eeden, F., Sealy, I., White, R. J., Herd, C., Nijman, I. J., et**
896 **al.** (2013). A systematic genome-wide analysis of zebrafish protein-coding
897 gene function. *Nature* **496**, 494-497. doi: 10.1038/nature11992.
898 **Kimmel, C. B., Ballard, W. W., Kimmel, S. R., Ullmann, B. and Schilling, T. F.**
899 (1995). Stages of embryonic development of the zebrafish. *Dev Dyn* **203**, 253-
900 310. doi: 10.1002/aja.1002030302.
901 **Kissa, K. and Herbomel, P.** (2010). Blood stem cells emerge from aortic
902 endothelium by a novel type of cell transition. *Nature* **464**, 112-115. doi:
903 10.1038/nature08761.
904 **Klepikova, A. V., Kasianov, A. S., Gerasimov, E. S., Logacheva, M. D. and**
905 **Penin, A. A.** (2016). A high resolution map of the Arabidopsis thaliana
906 developmental transcriptome based on RNA-seq profiling. *Plant J*. doi:
907 10.1111/tpj.13312.
908 **Kok, F. O., Shin, M., Ni, C. W., Gupta, A., Grosse, A. S., van Impel, A.,**
909 **Kirchmaier, B. C., Peterson-Maduro, J., Kourkoulis, G., Male, I., et al.**
910 (2015). Reverse genetic screening reveals poor correlation between
911 morpholino-induced and mutant phenotypes in zebrafish. *Dev Cell* **32**, 97-108.
912 doi: 10.1016/j.devcel.2014.11.018.

913 **Lee, M. T., Bonneau, A. R., Takacs, C. M., Bazzini, A. A., DiVito, K. R., Fleming,**
914 **E. S. and Giraldez, A. J.** (2013). Nanog, Pou5f1 and SoxB1 activate zygotic
915 gene expression during the maternal-to-zygotic transition. *Nature* **503**, 360-
916 364. doi: 10.1038/nature12632.
917 **Leichsenring, M., Maes, J., Mossner, R., Driever, W. and Onichtchouk, D.**
918 (2013). Pou5f1 transcription factor controls zygotic gene activation in
919 vertebrates. *Science* **341**, 1005-1009. doi: 10.1126/science.1242527.
920 **Li, P., Lahvic, J. L., Binder, V., Pugach, E. K., Riley, E. B., Tamplin, O. J.,**
921 **Panigrahy, D., Bowman, T. V., Barrett, F. G., Heffner, G. C., et al.** (2015).
922 Epoxyeicosatrienoic acids enhance embryonic haematopoiesis and adult
923 marrow engraftment. *Nature* **523**, 468-471. doi: 10.1038/nature14569.
924 **Liang, H. L., Nien, C. Y., Liu, H. Y., Metzstein, M. M., Kirov, N. and Rushlow, C.**
925 (2008). The zinc-finger protein Zelda is a key activator of the early zygotic
926 genome in Drosophila. *Nature* **456**, 400-403. doi: 10.1038/nature07388.
927 **Lindeman, L. C., Winata, C. L., Aanes, H., Mathavan, S., Alestrom, P. and**
928 **Collas, P.** (2010). Chromatin states of developmentally-regulated genes
929 revealed by DNA and histone methylation patterns in zebrafish embryos. *Int J*
930 *Dev Biol* **54**, 803-813. doi: 10.1387/ijdb.103081ll.
931 **Moens, C. B., Donn, T. M., Wolf-Saxon, E. R. and Ma, T. P.** (2008). Reverse
932 genetics in zebrafish by TILLING. *Brief Funct Genomic Proteomic* **7**, 454-459.
933 doi: 10.1093/bfgp/eln046.
934 **Murphey, R. D., Stern, H. M., Straub, C. T. and Zon, L. I.** (2006). A chemical
935 genetic screen for cell cycle inhibitors in zebrafish embryos. *Chem Biol Drug*
936 *Des* **68**, 213-219. doi: 10.1111/j.1747-0285.2006.00439.x.
937 **Nepal, C., Hadzhiev, Y., Previti, C., Haberle, V., Li, N., Takahashi, H., Suzuki, A.**
938 **M., Sheng, Y., Abdelhamid, R. F., Anand, S., et al.** (2013). Dynamic
939 regulation of the transcription initiation landscape at single nucleotide
940 resolution during vertebrate embryogenesis. *Genome Res* **23**, 1938-1950. doi:
941 10.1101/gr.153692.112.
942 **North, T. E., Goessling, W., Walkley, C. R., Lengerke, C., Kopani, K. R., Lord, A.**
943 **M., Weber, G. J., Bowman, T. V., Jang, I. H., Grosser, T., et al.** (2007).
944 Prostaglandin E2 regulates vertebrate haematopoietic stem cell homeostasis.
945 *Nature* **447**, 1007-1011. doi: 10.1038/nature05883.
946 **Owens, N. D., Blitz, I. L., Lane, M. A., Patrushev, I., Overton, J. D., Gilchrist, M.**
947 **J., Cho, K. W. and Khokha, M. K.** (2016). Measuring Absolute RNA Copy
948 Numbers at High Temporal Resolution Reveals Transcriptome Kinetics in
949 Development. *Cell Rep* **14**, 632-647. doi: 10.1016/j.celrep.2015.12.050.
950 **Pauli, A., Valen, E., Lin, M. F., Garber, M., Vastenhouw, N. L., Levin, J. Z., Fan,**
951 **L., Sandelin, A., Rinn, J. L., Regev, A., et al.** (2012). Systematic
952 identification of long noncoding RNAs expressed during zebrafish
953 embryogenesis. *Genome Res* **22**, 577-591. doi: 10.1101/gr.133009.111.
954 **Peterson, R. T., Link, B. A., Dowling, J. E. and Schreiber, S. L.** (2000). Small
955 molecule developmental screens reveal the logic and timing of vertebrate
956 development. *Proc Natl Acad Sci U S A* **97**, 12965-12969. doi:
957 10.1073/pnas.97.24.12965.
958 **Peterson, R. T., Shaw, S. Y., Peterson, T. A., Milan, D. J., Zhong, T. P.,**
959 **Schreiber, S. L., MacRae, C. A. and Fishman, M. C.** (2004). Chemical
960 suppression of a genetic mutation in a zebrafish model of aortic coarctation.
961 *Nat Biotechnol* **22**, 595-599. doi: 10.1038/nbt963.

962 **Petryszak, R., Keays, M., Tang, Y. A., Fonseca, N. A., Barrera, E., Burdett, T.,**
963 **Fullgrabe, A., Fuentes, A. M., Jupp, S., Koskinen, S., et al.** (2016).
964 Expression Atlas update--an integrated database of gene and protein
965 expression in humans, animals and plants. *Nucleic Acids Res* **44**, D746-752.
966 doi: 10.1093/nar/gkv1045.
967 **Potok, M. E., Nix, D. A., Parnell, T. J. and Cairns, B. R.** (2013). Reprogramming
968 the maternal zebrafish genome after fertilization to match the paternal
969 methylation pattern. *Cell* **153**, 759-772. doi: 10.1016/j.cell.2013.04.030.
970 **Rauch, G. J., Lyons, D. A., Middendorf, I., Friedlander, B., Arana, N., Reyes, T.**
971 **and Talbot, W. S.** (2003). Submission and Curation of Gene Expression
972 Data. ZFIN Direct Data Submission (http://zfin.org/). doi:
973 **Sheppard, S., Lawson, N. D. and Zhu, L. J.** (2013). Accurate identification of
974 polyadenylation sites from 3' end deep sequencing using a naive Bayes
975 classifier. *Bioinformatics* **29**, 2564-2571. doi: 10.1093/bioinformatics/btt446.
976 **Stern, H. M., Murphey, R. D., Shepard, J. L., Amatruda, J. F., Straub, C. T., Pfaff,**
977 **K. L., Weber, G., Tallarico, J. A., King, R. W. and Zon, L. I.** (2005). Small
978 molecules that delay S phase suppress a zebrafish bmyb mutant. *Nat Chem*
979 *Biol* **1**, 366-370. doi:
980 **Tan, M. H., Au, K. F., Yablonovitch, A. L., Wills, A. E., Chuang, J., Baker, J. C.,**
981 **Wong, W. H. and Li, J. B.** (2013). RNA sequencing reveals a diverse and
982 dynamic repertoire of the Xenopus tropicalis transcriptome over development.
983 *Genome Res* **23**, 201-216. doi: 10.1101/gr.141424.112.
984 **Theocharidis, A., van Dongen, S., Enright, A. J. and Freeman, T. C.** (2009).
985 Network visualization and analysis of gene expression data using BioLayout
986 Express(3D). *Nat Protoc* **4**, 1535-1550. doi: 10.1038/nprot.2009.177.
987 **Thisse, B., Pflumio, S., Fürthauer, M., Loppin, B., Heyer, V., Degrave, A., Woehl,**
988 **R., Lux, A., Steffan, T., Charbonnier, X. Q., et al.** (2001). Expression of the
989 zebrafish genome during embryogenesis. (NIH RO1 RR15402-01). ZFIN
990 Direct Data Submission (http://zfin.org/). doi:
991 **Tobin, D. M., Vary, J. C., Jr., Ray, J. P., Walsh, G. S., Dunstan, S. J., Bang, N. D.,**
992 **Hagge, D. A., Khadge, S., King, M. C., Hawn, T. R., et al.** (2010). The lta4h
993 locus modulates susceptibility to mycobacterial infection in zebrafish and
994 humans. *Cell* **140**, 717-730. doi: 10.1016/j.cell.2010.02.013.
995 **Ulitsky, I., Shkumatava, A., Jan, C. H., Subtelny, A. O., Koppstein, D., Bell, G.**
996 **W., Sive, H. and Bartel, D. P.** (2012). Extensive alternative polyadenylation
997 during zebrafish development. *Genome Res* **22**, 2054-2066. doi:
998 10.1101/gr.139733.112.
999 **van Dongen, S.** (2000). Graph Clustering by Flow Simulation. University of
1000 Utrecht.
1001 **Van Slyke, C. E., Bradford, Y. M., Westerfield, M. and Haendel, M. A.** (2014). The
1002 zebrafish anatomy and stage ontologies: representing the anatomy and
1003 development of Danio rerio. *J Biomed Semantics* **5**, 12. doi: 10.1186/2041-
1004 1480-5-12.
1005 **Varshney, G. K., Pei, W., LaFave, M. C., Idol, J., Xu, L., Gallardo, V., Carrington,**
1006 **B., Bishop, K., Jones, M., Li, M., et al.** (2015). High-throughput gene
1007 targeting and phenotyping in zebrafish using CRISPR/Cas9. *Genome Res* **25**,
1008 1030-1042. doi: 10.1101/gr.186379.114.
1009 **Vastenhouw, N. L., Zhang, Y., Woods, I. G., Imam, F., Regev, A., Liu, X. S., Rinn,**
1010 **J. and Schier, A. F.** (2010). Chromatin signature of embryonic pluripotency is

1011 established during genome activation. *Nature* **464**, 922-926. doi:
1012 10.1038/nature08866.
1013 **Wagner, E. J. and Carpenter, P. B.** (2012). Understanding the language of Lys36
1014 methylation at histone H3. *Nat Rev Mol Cell Biol* **13**, 115-126. doi:
1015 10.1038/nrm3274.
1016 **Yang, H., Zhou, Y., Gu, J., Xie, S., Xu, Y., Zhu, G., Wang, L., Huang, J., Ma, H.**
1017 **and Yao, J.** (2013). Deep mRNA sequencing analysis to capture the
1018 transcriptome landscape of zebrafish embryos and larvae. *PLoS One* **8**,
1019 e64058. doi: 10.1371/journal.pone.0064058.
1020